

Automatic classification and mapping of the seabed using airborne LiDAR bathymetry

Lukasz Janowski^{a,*}, Radoslaw Wroblewski^{b,c}, Maria Rucinska^d,
Agnieszka Kubowicz-Grajewska^d, Pawel Tysiac^{e,f}

^a Maritime Institute, Gdynia Maritime University, Dlugi Targ 41/42, 80-830 Gdansk, Poland

^b Institute of Geography, University of Gdansk, ul. Bazynskiego 4, 80-309 Gdansk, Poland

^c MEWO S.A, Starogardzka 16, 83-010 Straszyn, Poland

^d Institute of Oceanography, University of Gdansk, al. Marszalka Pilsudskiego 46, 81-378 Gdynia, Poland

^e Faculty of Civil and Environmental Engineering, Gdansk University of Technology, Gabriela Narutowicza 11/12, 80-233 Gdansk, Poland

^f Apeks Company Ltd., Jaskowa Dolina 81, 80-286 Gdansk, Poland

ARTICLE INFO

Keywords:

Airborne LiDAR bathymetry
Underwater bottom topography
Bedform classification
Coastal protection structures
Sustainable management
GEOBIA

ABSTRACT

Shallow coastal areas are among the most inhabited areas and are valuable for biodiversity, recreation and the economy. Due to climate change and sea level rise, sustainable management of coastal areas involves extensive exploration, monitoring, and protection. Current high-resolution remote sensing methods for monitoring these areas include bathymetric LiDAR. Therefore, this study presents a novel methodological approach to assess the suitability of Airborne LiDAR Bathymetry for automatic classification and mapping of the seafloor. Nine classes of geomorphological bedforms and three classes of anthropogenic structures were identified. They were automatically mapped by Geographic Object-Based Image Analysis and machine learning supervised classifiers. The developed method was applied to six study sites and a 48 km submerged coastal zone in the Southern Baltic, achieving an overall accuracy of up to 94%. This study shows that calculation of the Multiresolution Index of Ridge Top Flatness (secondary feature) can be used to quickly and automatically determine sandbar crests and ridge tops. The methodical approach developed in this study can help evaluate and protect other shallow coastal environments and coastal protection structures.

1. Introduction

The expansion of human activity to coastal areas leads to an intensification of the economic, tourist, and recreational use of these areas. Therefore, information is needed on the conditions, development and functioning of these areas. Today, coastal administrations and the coastal community face the challenges of climate change, including sea level rise, intense coastal erosion, and flooding of low-lying coastal areas. The shallow coastal zone is characterised by a complex bathymetry. It includes many different-scale systems of nearshore bedforms that dynamically change at different spatial and temporal scales. In addition, sandbars are very important structures that cause waves to break. They are essential to protect coastal and beach areas from intense waves and currents, especially during storms. An important parameter for the condition of sandbars is their longshore integrity. In the event of

temporary damage to the sandbar system, sections of sandbars are exposed to increased energy transmission from the open sea to the shore. This therefore leads to increased erosion of the beach and coastline retreat. Identification of the bottom relief in the coastal zone allows assessment of dynamic coastal structures and description of their spatial stability and equilibrium state.

The geological-engineering aspects of the nearshore Baltic seabed sediments relate to geological factors such as lithology, origin and age of sediments, as well as geotechnical parameters: density index, consistency index, internal friction angle, cohesion, shear strength, and oedometric modulus. Due to the fact that geotechnical parameters can vary locally owing to different angles of inclination of the seabed surface, the classification of geomorphological forms is important. Furthermore, the upper 1.5–2.0 m layer of seabed sediment is continuously exposed to the impact of seawater. Depending on its composition,

* Corresponding author.

E-mail addresses: ljanowski@im.umg.edu.pl (L. Janowski), radoslaw.wroblewski@ug.edu.pl (R. Wroblewski), maria.rucinska@ug.edu.pl (M. Rucinska), agnieszka.kubowicz-grajewska@ug.edu.pl (A. Kubowicz-Grajewska), pawtysia@pg.edu.pl (P. Tysiac).

<https://doi.org/10.1016/j.enggeo.2022.106615>

Received 28 September 2021; Received in revised form 18 February 2022; Accepted 8 March 2022

Available online 12 March 2022

0013-7952/© 2022 The Authors. Published by Elsevier B.V. This is an open access article under the CC BY license (<http://creativecommons.org/licenses/by/4.0/>).

cohesive soils in the upper seabed can be in a soft or even liquid state, while in non-cohesive soils the seabed is fully saturated with seawater. A detailed study of local conditions is often required to assess the necessity and design of coastal protection.

Coastal mapping is one of the fundamental tools that support coastal engineering. It is an important element in monitoring and assessing the condition of both the shore and the coast. It allows the identification of areas most sensitive to changes caused by erosion, which enables effective and economical management of shore protection. In the case of protected shores, coastal mapping allows quick verification of the functionality and efficiency of the reinforcement applied, which further contributes to the improvement of engineering practice. Therefore, effective coastal management requires monitoring and mapping. This is a technical and logistic challenge (Wozencraft and Millar, 2005). It involves both an accurate and detailed exploration of coastal areas and a comprehensive spatial understanding of the processes occurring there. Bathymetric LiDAR (Light Detection and Ranging) surveys may provide such a possibility for shallow coastal areas.

The use of Airborne LiDAR Bathymetry (ALB) has become a widespread technology for high-resolution mapping of shallow areas (Wehr and Lohr, 1999). Compared to underwater acoustic systems, ALB is suitable for large areas, providing dense and accurate data (Schmidt et al., 2013). The experience gained by the Irish national mapping programme INFOMAR showed that, beyond hydroacoustics, bathymetric LiDAR provides an excellent source of high-resolution spatial data for the nearshore zone (Coveney and Monteys, 2011). Furthermore, time series of ALB datasets can successfully support accurate change detection analysis in this challenging environment (Robertson et al., 2018).

In recent years, aerial remote sensing has been applied in various types of research related to water and coastal areas. LiDAR technology enables very precise determination of water depth, useful for coastal monitoring and protection (Tysiac, 2020). LiDAR bathymetry relies on wavelengths (spectra) of the visible spectrum, which are less absorbed by water. Longer wavelengths are absorbed faster as they travel through the water column, while shorter wavelengths penetrate at greater depths. Water penetration at different wavelengths is further affected by the content of substances, such as chlorophyll and suspended solids, which absorb certain wavelengths (Kutser et al., 2006). The approach to bathymetry determination is often referred to as describing methods for taking measurements (Genchi et al., 2015) or optimising their processing (Guo et al., 2021). One of the contributions of this research is to propose a specific solution for the classification of morphological forms, whose continuous monitoring improves the quality of coastal protection. With regard to the classification of seafloor relief, bathymetric LiDAR has not been widely used to date. The technology is expensive and generates an enormous amount of data (Tysiac, 2020). Potential applications available in the literature include monitoring of shallow coastal areas (Cottin et al., 2014), classification of tidal environment (Andersen et al., 2017), benthic habitat mapping (Collin et al., 2008), monitoring of the condition of navigation channels and protective structures (Wozencraft and Millar, 2005), geomorphology (Xhardé et al., 2011), organisation and distribution of archaeological sites in shallow water (Doneus et al., 2015). Moreover, sedimentological (density, compaction) and hydrodynamical (suspended sediment concentration, turbulence) information was acquired from ALB based on the analysis of laser return intensity waveforms (Long et al., 2011). It was noted, however, that the available publications that refer to small coastal areas are based on studies conducted several years ago.

Airborne measuring systems enable much faster surveys in shallow areas compared to acoustic systems. The use of airborne measurement techniques reduces the cost of mapping large coastal areas. Hydro-acoustic measurements are often assumed to fill gaps in airborne data coverage as there are many features that relate to water penetration by the laser beam, e.g. siltation, disturbance level, water level, type of scanning system, and signal processing methods. Various applications

were presented by Lague and Feldmann (2020), who identified the applicability of solutions in terms of geometric changes, calculation of optical properties of points, or high-resolution mapping methods. The presented solutions are strictly engineering solutions. As a consequence, there are gaps in the literature regarding the classification of morphological forms with the use of ALB.

The identification and classification of seabed geomorphology from remote sensing datasets can be performed based on several approaches, for example with the support of additional morphometric features or backscatter intensity measurements. The whole procedure is performed manually and involves expert knowledge by preferably a single interpreter (Diesing et al., 2016). The generation of manual maps is therefore labour intensive and time consuming. Automatic or semi-automatic methods of seabed classification, on the other hand, consist of unsupervised or supervised approaches. In the first approach, the seafloor is extracted based on properties and relationships within the remote sensing dataset (e.g., unsupervised Jenks classifier; see Fogarin et al., 2019). The second approach involves training a classifier with a ground-truth input dataset that can be determined manually or in the field (Brown et al., 2011). Both techniques can be applied in pixel-based or geographic object-based image analysis. The latter was used in seafloor research for more than ten years (Lucieer, 2008).

So far, geomorphological assessment and high-resolution maps of Polish shallow waters have been available only for dispersed and isolated areas. The sources of these data were: discrete sediment collections, in situ measurements, singlebeam echosounder profiles, MBES, or bathymetric LiDAR (Tysiac, 2020). Recent nearshore data shared by the Maritime Office in Gdynia have provided a unique opportunity to understand and validate the usefulness of ALB data for geomorphological studies. As an inland sea with relatively low water exchange with the ocean, the Baltic Sea requires constant monitoring (Reusch et al., 2018). Destructive wave action and climate change are one of the main challenges facing the Baltic Sea and the proper development of its coastal regions (Kundzewicz et al., 2018).

Analysis of the dynamics of coastal changes in the Southern Baltic Sea in the late 19th and 20th century indicated an increase in erosion phenomena. In recent decades, the frequency of storm surges has increased due to changes in atmospheric circulation (Pruszk and Zawadzka, 2008). These phenomena have exacerbated erosional changes and necessitated larger-scale monitoring using LIDAR technology. In Poland, airborne surveys conducted as part of the coastal monitoring programme of the Maritime Office in Gdynia have largely filled the gap of high-resolution maps of the shallowest Polish waters. The availability of such datasets provides the first opportunity to accurately identify and classify the existing bedforms. This task is essential for environmental policy management, sustainable development, coastal protection, and decision-making. Furthermore, to our knowledge, this study represents one of the first high-resolution ALB assessment approaches to the identification, classification, and automatic mapping of natural bedforms and coastal engineering structures. The execution of this demanding task required the pursuit of more specific research objectives.

The following research objectives were addressed in this study: (a) identification and classification of geomorphological bedforms occurring in both natural and anthropogenic sections of the coastal zone of the Southern Baltic; (b) development of an accurate automatic mapping method for geomorphological bedforms and coastal protection structures based on topo-bathymetric LiDAR measurements; (c) comparison of machine learning classification results with manual characterisation of seabed forms and coastal protection structures; (d) determination of a predictor variable suitable for automatic delineation of sandbar crests; (e) evaluation of machine learning classification procedures for ALB areas without previous manual identification.

2. Materials and methods

2.1. Study sites

The study area is located in the Polish coast of the Southern Baltic, exposed to increased coastal erosion (Musielak et al., 2017). Recognising the challenges associated with coastal protection, the Maritime Office in Gdynia commissioned a topo-bathymetric airborne LiDAR survey as part of the coastal monitoring programme. The dataset from 2020 is the first high-resolution wide-range bathymetry acquired using the LiDAR technique in the very shallow nearshore zone of the Polish coast of the Southern Baltic. The study area is a 48 km section of the Polish coastal zone of the Southern Baltic Sea, managed by the Maritime Office in Gdynia (Fig. 1). The Baltic Sea is a relatively small, basically nontidal (6 cm range in Poland) body of water, connected with the North Sea by the narrow and shallow Danish Straits. The Polish coast is about 500 km long, and the geomorphology and geology of its shores are associated with the last glaciation and development phases of the Southern Baltic Sea (Pruszek and Zawadzka, 2008).

There are mainly two natural types of seashore: cliffs and dunes. Cliff shores constitute about 20% of the entire coastline length, whereas dune shores account for more than 75%. The remaining small part is occupied by coastal wetlands (Dubrawski and Zawadzka-Kahlau, 2006). Dune coasts are primarily composed of modern aeolian and marine sands overlying Holocene dammed-lake deposits and/or Pleistocene fluvio-glacial and glacial deposits. Cliffs are composed mainly of Pleistocene glacial and fluvio-glacial sediments with a thin cover of Holocene sediments – dammed-lake and lacustrine silts and clays with occasional aeolian sands.

The nearshore zone to a depth of approximately 10 m consists mainly of fine-grained sands. Coarse-grained sediments occur locally in the

vicinity of abraded cliffs. Recent marine sediments directly overlie Pleistocene deposits (Uściniowicz, 2011). The nearshore profile often include 2–5 sandbars aligned approximately parallel to the shore. The sandbar closest to the shore develops at a depth of 0.5–1.5 m, ranging from 500 m to 1200 m, whereas the outermost sandbar develops at approximately 8.0–9.0 m. The selected sites are seabed strips extending from the shoreline to a depth of approximately 5.5 m. They are located within the sandbar zone of dune coasts.

Study sites N1, N2, N3 and N4 are associated with natural sections of the shoreline, whereas study sites A1 and A2 are associated with anthropogenically modified coastal areas in close vicinity of the towns of Rowy and Ustka (Fig. 1). In the latter, three types of coastal protection structures were used simultaneously: groynes, submerged breakwaters, and artificial reef modules.

2.2. Engineering geology aspects of the study area

Spatial distribution of the main sediments covering the study area is presented in Fig. 2. According to the estimates provided in Kaszubowski and Coufal (2010), the engineering geology parameters of fine and gravelly sands occurring here are within the following range: degree of compaction – approx. 0.5, angle of internal friction $<30^\circ$, shear strength – 300–350 MPa, primary oedometric modulus – 80–100 MPa. Because sediment stability is directly related to slope, inspired by Kaszubowski and Coufal (2010), we implemented a local seafloor morphology assessment based on slope values to assess the necessity of coastal protection. The scale used is as follows: 1) flat bottom $<0.5^\circ$, inclined bottom 0.5–1.5°, low steep bottom 1.5–3°, steep bottom 3–5°, high steep bottom 5–10°, very steep bottom $>10^\circ$.

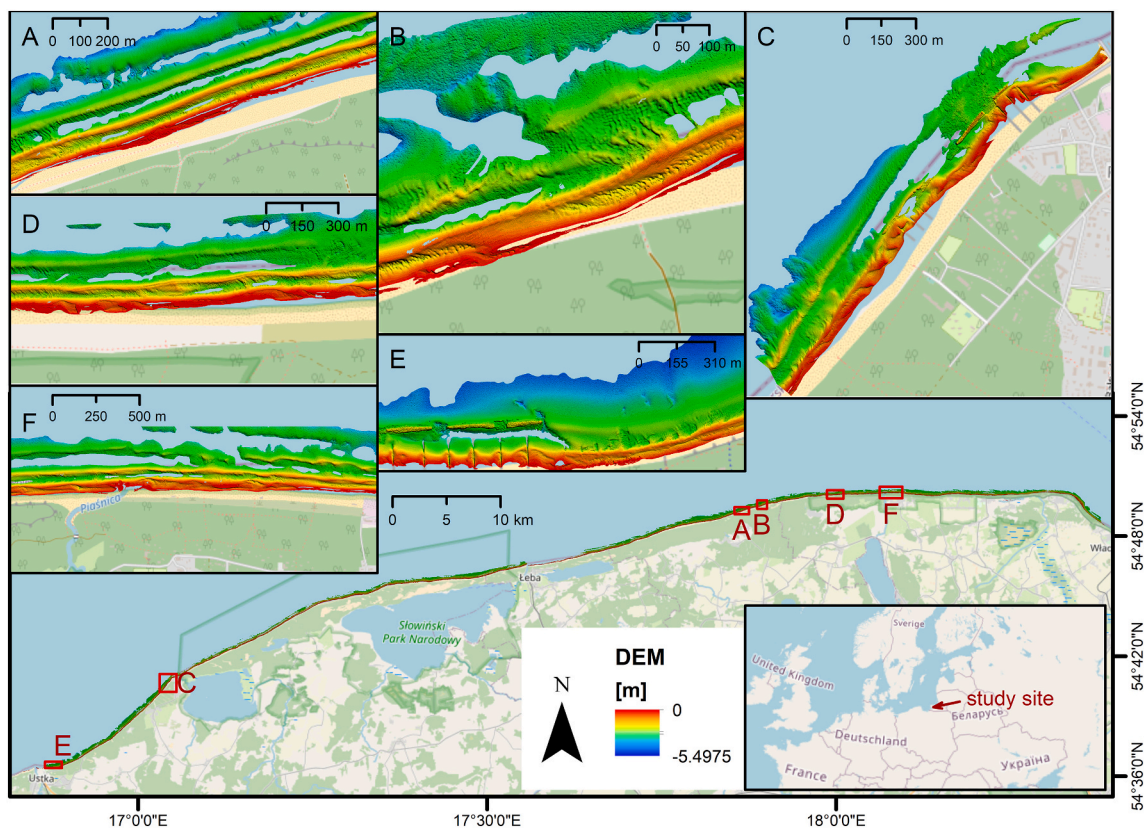


Fig. 1. Location of the study sites within the Polish coast of the Southern Baltic (size of the sites provided in brackets). A – study site N1 (0.90 km²); B – study site N2 (0.71 km²); C – study site A1 (2.62 km²); D – study site N3 (1.19 km²); E – study site N4 (0.93 km²); F – study site A2 (2.23 km²). Original ALB DEM provided by the Maritime Office in Gdynia. Basemap: Openstreetmap.

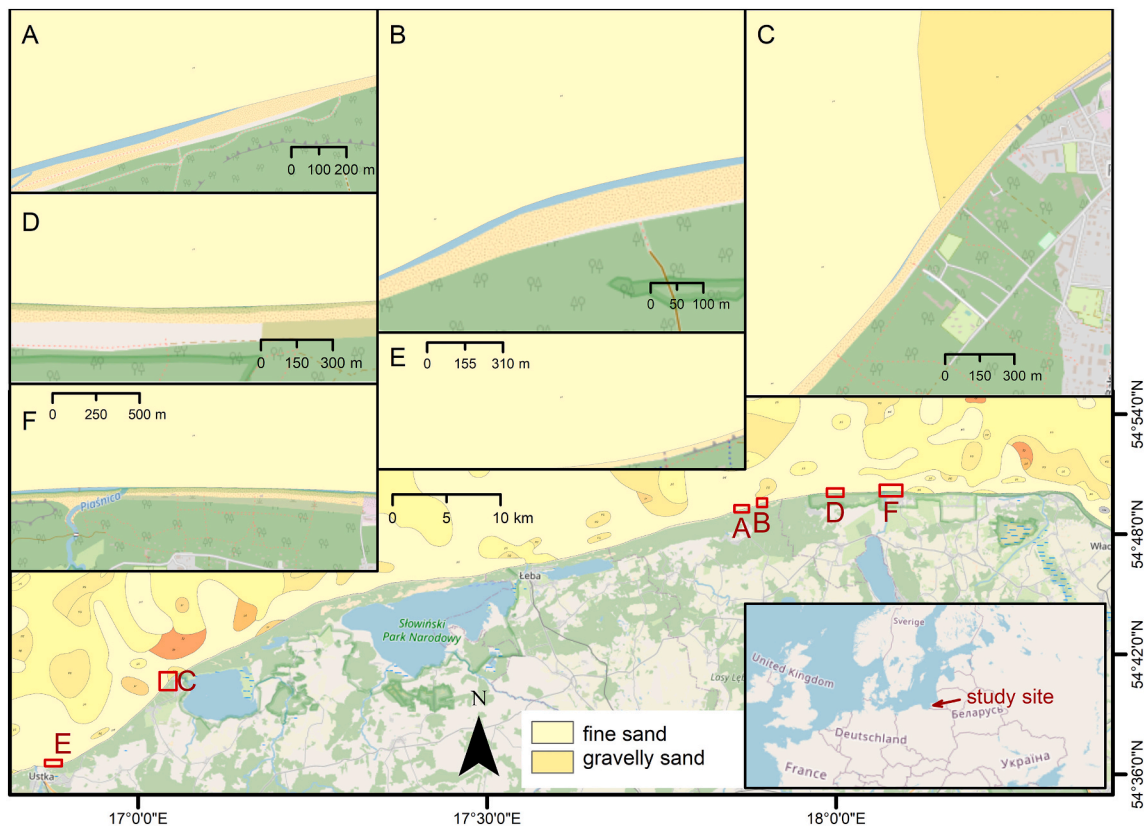


Fig. 2. Sediments occurring at the study sites. A – study site N1; B – study site N2; C – study site A1; D – study site N3; E – study site N4; F – study site A2. Basemap dataset: Geological map of the Polish maritime areas at a scale of 1:200,000. Polish Geological Institute – National Research Institute.

2.3. Data acquisition and processing

The ALB data were provided by the Opegięka Company (HQ: Elbląg, Poland). Table 1 shows the instruments and software used in the experiment. At the request of the Maritime Office in Gdynia, the contractors provided technical reports from the conducted survey (Maritime Office in Gdynia, 2020). These included measurement equipment, statistical values for trajectory alignment and average point density from the bathymetric scanner. Table 1 presents a summary of this information.

The measurement capabilities are described in the manufacturer's specification (Riegl, 2019) and in Tysiac (2020), referring to direct measurement possibilities in the Baltic Sea. It follows from these references that an appropriate flight should be performed in accordance with technical standards while maintaining the best detail of data. Data

Table 1 Instruments and software used by the Maritime Office in Gdynia (Maritime Office in Gdynia, 2020) for data acquisition.

Instruments	Specifications	Software	Manufacturer
Plane: Vulcanair P68 TC Observer – Flight Execution	–	RAW Point Cloud processing: SDCImport 3.0, RiWORLD v6.0, RiProcess v1.8.6, RiHydro v1.8.5	Riegl GmbH, Horn, Austria
Bathymetry Laser Scanner: Riegl VQ-1560i-DW	Average scanning density: 2×12.4 points/m ²	Point Cloud postprocessing: Microstation V8i + TerraScan and TerraModeler	Bentley, Pennsylvania, USA Terrasolid Ltd., Helsinki, Finland
Navigation: GPS- IMU Applanix AP	Accuracy: XY: 0.02 m Z: 0.07 m	Trajectory adjustment: PosPac	Applanix, Richmond Hill, Canada

records from the ALB must be performed with the required accuracy.

It should be noted here that water siltation has not been taken into account (according to Riegl, 2019, the scanner can register points down to a depth of 0.7 Secchi). Therefore, the Riegl VQ-1560i-DW bathymetric scanner may not provide complete spatial data on the seabed. There is a possibility that artefacts consist of too high beam absorption in water, so there is no point registration. The entire research process is presented in Fig. 3. Processing of airborne scanner data included preparation of raw ALB data, data alignment without manually measured control points, adjustment of the point cloud to the ground control network, followed by automatic classification, manual classification, Digital Elevation Model (DEM) building, and data control.

A geodetic network was used to georeference the point cloud. The alignment is based on control planes that allow point cloud geometry calibration. The observed and measured systematic errors are converted into shift vectors. The RiProcess software calculates and corrects systematic errors such as shift, drift in all directions (XYZ) together with yaw, roll, and pitch angles. Using a control network in the form of reference planes, the point cloud displacement vector is determined to optimise its position. The study used nine reference objects designed along the flightlines. The reference object consists of roof slope. For each roof slope, a theoretical roof plane was fitted into the point cloud. The plane fitted by the point cloud was then compared with the plane formed by the measured ground points. For each slope, a vector was calculated to determine the shift between field measurements and the point cloud.

In the processing of bathymetry data, two physical phenomena were taken into account to obtain reliable results:

- refraction of the radiation beam passing through the water surface;
- lower speed of the laser beam propagation in the water medium.

Accounting for the effects of the above-mentioned physical

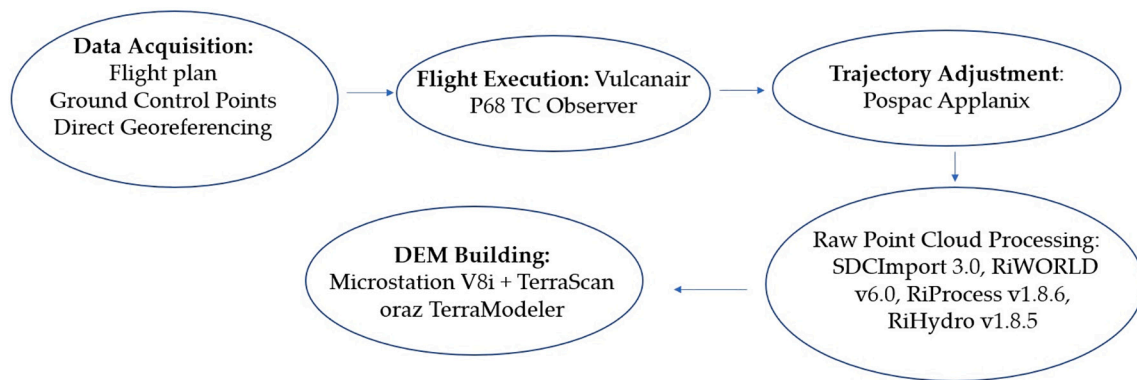


Fig. 3. Point cloud processing scheme.

phenomena is referred to as “refractive correction”. To this end, a Water Surface Model (WSM) was created for each series of points defining the water surface. Based on the WSM model, a refraction correction was applied to the data defining the bottom rebound using Riegl’s RiHydro tool. The TerraScan and TerraModeler software were used to build a DEM.

The airborne LiDAR bathymetry grids provided by the Maritime Office in Gdynia are available as raster grids with $0.5\text{ m} \times 0.5\text{ m}$ spatial resolution. The depth of the original LiDAR DEM grid was limited from the deepest range of -8.5 m to 0 m . For the sake of data quality, we removed the most visible triangular interpolation artefacts that were introduced to fill gaps in the original LiDAR DEM data coverage. To this end, we exposed the triangular interpolation artefacts by extracting the hillshade feature of the DEM in ArcGIS software (manufactured by Environmental Systems Research Institute ESRI). Hillshade was then segmented using multiresolution segmentation in eCognition software (working principles of the segmentation algorithm are described in the following section of this article). The resulting segments with a relatively low mean standard deviation of hillshade (lower than 1.2–1.4) were then classified as triangular artefacts. The resulting DEMs were further refined manually to remove triangulation residues. The ALB grids processed in this way had gaps in spatial coverage compared to the original rasters. In return, the quality of DEM was much improved, so we could be confident that further stages of the automatic classification would not be affected by errors resulting from significant triangular interpolation artefacts.

2.4. Data analysis

2.4.1. Manual investigation and interpretation of bedforms

Detailed manual investigation of bedforms involved the analysis of seafloor relief by delineating boundaries of bedforms based on the interpretation of depth, slope, and aspect (including delineation of edges, slope bases, bedform ridges, and trough forms axes). The analysis was based on bathymetry derived at a scale of 1:5000 or greater. The slope, aspect and bathymetric profiles were generated using Global Mapper 21.1 software (manufactured by Blue Marble Geographics).

Nine types of bedforms and three types of anthropogenic objects were distinguished. Prior to manual interpretation of the data, the most visible triangular interpolation artefacts were removed, although small interpolation residues still remained. We included them in the separate class, named artefacts (class 1, Table 2). Similarly, some geomorphological classes were separated into bedforms as well as bedforms with artefacts (Table 2). Sandbars and interbar depressions are characterised by an irregular pattern of rises and depressions forming an undulating seabed (classes 2 and 3). Risings range from 0.3 to 0.5 m above the surrounding seabed, with distances between the forms ranging from 10.0 to 40.0 m. Each study site consists of sandbars with relatively smooth top surfaces and distal slopes (classes 4 and 5). The seabed often

includes many irregularities of varying sizes between the first sandbar and the shore (class 6) and interbar depressions (class 7). Residual traces of microforms usually cover the rough surface of the latter. Classes 8 and 9 represent bedforms that form a pattern indicating the flow of water parallel to the shore (Table 2). Linguoid ripples have a spacing of 2.0 to 7.0 m and a height of 0.2 to 0.3 m (maximum up to 0.5 m). Straight or sinuous ripples are characterised by a ripple crest spacing of 2.0 to 5.0 m (maximum 12.0 m) and a ripple height of 0.2 to 0.4 m (maximum up to 0.5 m).

Groynes are located only at study sites A1–A2 (class 10). These structures are perpendicular to the shore and built of wooden piles with a diameter of $\sim 0.25\text{--}0.4\text{ m}$ and an elevation of $+0.6\text{ m}$ above sea level. They are 150 m long with a 60 m spacing at study site A1 and a 180 m long and 110 m spacing at study site A2. The submerged breakwaters are constructed of granite blocks with gaps between the segments filled with habitat modules (class 11). Habitat modules are also found at the ends of submerged breakwaters. The last type of hard construction found in the study area are concrete modules arranged in trapezoidal form in the spaces between the submerged breakwaters and at their ends (class 12). In the head area, the modules form reinforced concrete circles with an internal diameter of 2 m, a height of 1.5, 2.0, and 2.5 m (adjusted to the depth of the water body in the area). The module surface consists of many inlet openings, with the main outlet opening located in the upper surface. The modules are arranged with a spacing of $4 \times 4\text{ m}$. The maximum depth of the upper part of the element to the water level is 1.2 m. Class 13 was found only at study site A2. It is a flat surface between the first bar and the shore built of strongly compressed peat. Its identification was possible on the basis of the interpretation of LiDAR data, an orthophotomap, and fieldwork at this study site. The identified distinct bedform areas are presented in terms of seabed surface characteristics in Table 2. Table 3 shows the parameters of the submerged breakwaters located at the artificial study sites (A1–A2).

Interpretation and manual classification also included the determination of sandbar crests for the selected study site (N1; Fig. 1A). Sandbar crests are represented by lines indicating the highest tops of underwater sandbars in the coastal/sandbar zone. They were manually digitised on the basis of the DEM, hillshade, slope, and aspect features. They were determined as the highest parts of the ridges and the areas with clearly the largest changes in aspect. We assumed a 5 m cross-sectional width range of sandbar crests to replace lines with the study sites.

2.4.2. Feature extraction and selection

Automatic processing of the ALB datasets consisted of the following steps: 1) feature extraction and selection, 2) determination of ground-truth control points, 3) GEOBIA (Geographic Object-Based Image Analysis) image segmentation and classification, 4) map generalisation, 5) accuracy assessment. The following sections describe details of the above-mentioned steps.

The DEM processed in the previous step formed the basis for

Table 2
List of the identified and classified bedforms and anthropogenic objects with their description.

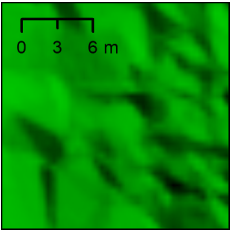
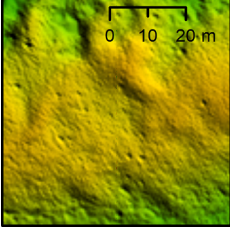
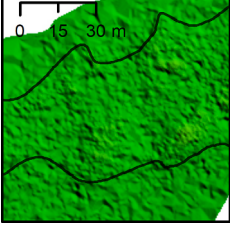
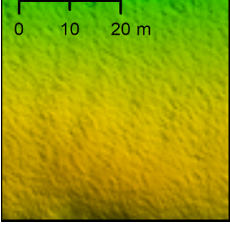
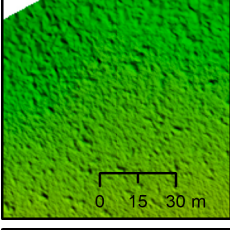
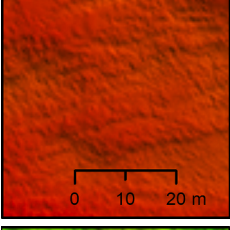
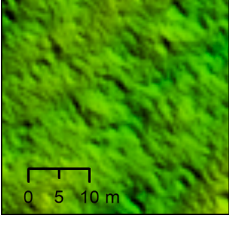
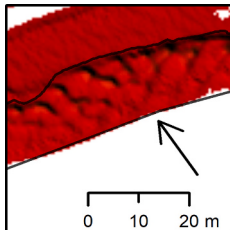
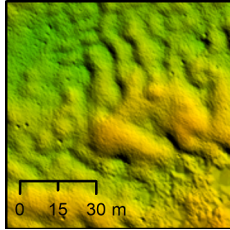
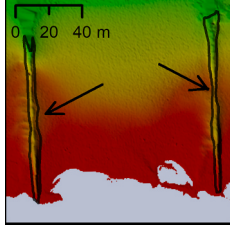
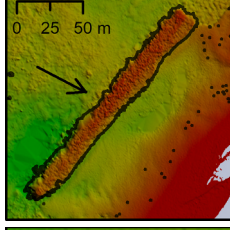
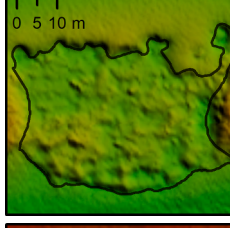
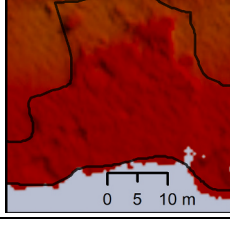
No.	Bathymetry	Name	Description
1		Artefacts	Seabed areas with visible interpolation residues
2		Undulating bed	Slightly undulating sandy seafloor area within sandbars and depressions between them
3		Undulating bed with artefacts	The same surface character as in unit 2, but with artefact disturbances
4		Plain bed	Levelled surface of sandy bottom, mainly tops of bars and distal slopes of bars
5		Plain bed with artefacts	The same surface character as in unit 4, but with artefact disturbances
6		Other irregularities	Irregularities of the bottom surface forming a chaotic pattern of small hills and depressions
7		Uneven trough bed	Rough bottom surface usually in interbar depressions with residual traces of microforms
8			

Table 2 (continued)

No.	Bathymetry	Name	Description
		Linguoid (tongue-shaped) ripples	Ripples usually in a pattern indicating water flow parallel to the shore
9		Straight or sinuous ripples	Large ripples usually in a pattern indicating water flow parallel to the shore
10		Groynes	Groynes perpendicular to the shore built of wooden piles
11		Submerged breakwaters	Submerged breakwaters built of granite blocks with habitat modules
12		Artificial reef modules	Concrete modules arranged in trapezoid form in the spaces between submerged breakwaters and at their ends
13		Peat	Flat surface between the first bar and the shore built of strongly compressed peat

extracting secondary features (also known as derivatives, geomorphic attributes, or predictor variables). They include simple statistics of ALB, like standard deviation and variance, geomorphometric attributes, like aspect (maximum downslope direction), slope (in degrees), and curvature (slope of slope), and more advanced derivatives, based on i.a. geometric properties of the surface (morphometric features), machine vision approach (geomorphons), slope and curvature properties (Fuzzy Landform Element Classification). Table 4 presents the list of all 21 predictor variables. They were extracted using ArcGIS 10.8 and SAGA (System for Automated Geoscientific Analyses) 7.9.0 software.

The extracted features may provide relevant ecological and

Table 3
Parameters of submerged breakwaters located at study sites A1–A2.

Submerged breakwaters parameters	Rowy (A1)	Ustka (A2)
Length	950 m (four segments 187.5 m long)	850 m (two segments 200 m long and two segments 150 m long)
Gap width	two segments 66 m wide and one 68 m wide	50 m
Distance from the shoreline	ca. 150 m	ca. 200–230 m
Crest submergence	−0.62 m b.s.l.	−0.62 m b.s.l.
Crest width/base width	6 m/22.6 m	6 m/22.6 m
Inclination of the landward and seaward escarpment	1:2/1:4	1:2/1:4

Table 4
List of all ALB geomorphic attributes extracted in this study.

ID	Feature	Software
1	Aspect	ArcGIS
2	Northness	ArcGIS
3	Eastness	ArcGIS
4	Slope	ArcGIS
5	Curvature	ArcGIS
6	Profile curvature	ArcGIS
7	Planar curvature	ArcGIS
8	Surface area to planar area	ArcGIS
9	Standard deviation of ALB	ArcGIS
10	Variance	ArcGIS
11	Vertical ruggedness measure (VRM)	ArcGIS
12	Curvature classification	SAGA GIS
13	Fuzzy Landform Element Classification	SAGA GIS
14	Geomorphons	SAGA GIS
15	Morphometric features	SAGA GIS
16	Multiresolution Index of Valley Bottom Flatness (MRVBF)	SAGA GIS
17	Multiresolution Index of Ridge Top Flatness (MRRTF)	SAGA GIS
18	Topographic Position Index (TPI)	SAGA GIS
19	Terrain Ruggedness Index (TRI)	SAGA GIS
20	Terrain Surface Classification Landforms	SAGA GIS
21	Terrain Surface Classification Convexity	SAGA GIS

geomorphological information. For example, as mentioned earlier, slope is a good predictor of sediment stability and local acceleration of currents, processes that have a strong impact on the formation of bedforms. The aspect is related to the general direction of geomorphic processes, and curvature can help to distinguish peaks or hollows that are more or less exposed to or sheltered from the water flow. The vertical ruggedness measure indicates the rugosity of the terrain that may result from the variability and biodiversity of the seafloor. The description of other geomorphic attributes can be found in the relevant software documentation and literature.

Feature selection refers to the selection of features (or derivatives/variables/attributes) that were extracted from the DEM and are suitable for automatic classification (Diesing et al., 2016). The features listed in Table 4 were tested in terms of their suitability to improve classification performance. We incorporated several approaches to feature selection, such as rejection of cross-correlated features, the Boruta algorithm for all relevant feature selection (Kursa and Rudnicki, 2016), and feature selection algorithms embedded in supervised classification algorithms (Breiman, 2001; Breiman et al., 1984). To find a minimum optimal number of features yielding the classification model with the best performance, the number of active variables was adjusted to the square root of all variables or the natural logarithm of all ground-truth control points. The implementation of the Boruta algorithm and the cross-correlation of features was performed in the R software (manufactured by the R Foundation for Statistical Computing), whereas implementations of the embedded feature selection were performed in the

eCognition software (manufactured by Trimble Inc.).

2.4.3. Determination and use of ground-truth control points

Manual maps of geomorphological bedforms were used to generate ground-truth control points (or samples). Control points were necessary to train the supervised classifiers and calculate the accuracy of the results. Ground-truth samples were determined in a random way using the Create Random Points tool in the ArcGIS software. They were generated within the study sites by manual classification with a minimum distance of 1 m for each point, not closer than 2–4 m from the boundaries of the study sites (2 m at study sites A1–A2). The number of control points (pixels) reached approximately 5000 for each study site. Their distribution between the bedform classes varied proportionally depending on the percentage aerial coverage of all units. In the case of minimal aerial coverage of some classes, such as anthropogenic objects, the number of samples was increased to 50 to ensure the statistical significance of future calculations. Ground-truth samples were divided into training and test subsets in a 70/30 ratio for each study site. The Subset Features tool in ArcGIS was used to perform this step in a random way.

Moreover, classification models were applied to the entire 48 km study area. For this purpose, supervised classifiers were trained and tested based on a total dataset of ground-truth samples from the four natural study sites (Fig. 1A, B, D, F). As one particular class of artefacts was only present at study sites N1 and N4, we combined the training and validation subsets from both study sites. The following description applies to the remaining samples from other bedform classes. In the first model (G1), all samples from N1/N3/N4 study sites were assigned to training, and the remaining samples from study site N2 were allocated to validate the model. In the latter approach (model G2), all samples from N1/N2/N4 study sites were selected for training, whereas the other samples from study site N3 were used for model testing.

2.4.4. Geographic object-based image analysis

GEOBIA is a widely used approach to remote sensing image analysis. It was developed over approximately two decades, mainly using the eCognition software (as in this study). Image segmentation and classification are the main components of the GEOBIA approach. The working principle of image segmentation is to separate images into homogenous segments (or image objects) with similar spectral properties, which can be used for further analysis instead of pixels. Due to the high-resolution of current remote sensing images, the most detailed measurements represented in pixel values can be disrupted by various environmental and physical factors, causing data artefacts. The GEOBIA approach enables the generation of image objects free of these artefacts, similar to human vision. In addition, image objects contain much more detailed information (like textural and shape characteristics) than pixels. The GEOBIA approach is recommended especially for high-resolution remote sensing images with heterogeneous pixel information (Blaschke, 2010).

Image objects were generated based on the multiresolution segmentation algorithm (Benz et al., 2004). The working principle of this approach is to merge image pixels with similar spectral properties constrained by several parameters – scale, shape, and compactness (Benz et al., 2004). After multiple tests, we evaluated the following settings of these parameters: scale 5, shape 0.1, compactness 0.1. The same settings were applied to all study sites based on two layers: DEM and Fuzzy Landform Element Classification with equal weights.

As each supervised classifier has its own specific strong and weak aspects, we tested different algorithms following the recommendations of Diesing et al. (2016). Image classifications were performed based on: K-Nearest Neighbour (KNN), Support Vector Machines (SVM), Classification and Regression Trees (CART; Breiman et al., 1984), and Random Forest (RF; Breiman, 2001). All classifiers were trained based on training sets of ground-truth samples and different sets of predictor variables, selected using the methods described in the previous paragraphs.

2.4.5. Map generalisation

The Polish Chief Inspectorate of Environmental Protection has set the initial requirement for the scale of seafloor maps at 1:25000. Since cartographers generally consider areas smaller than 2 mm as an error limit, we decided to eliminate areas smaller than 2×2 mm, adopting a scale of 1:10000, which was more accurate than the mentioned preliminary requirements. Therefore, once the resulting maps were obtained, the map generalisation approach was applied to improve the overall readability and quality of the classification results. Minor classification artefacts in areas smaller than 400 m² were merged into neighbouring classes. Map generalisation was performed using the Eliminate Study site Part algorithm in ArcGIS software.

2.4.6. Accuracy assessment

The accuracy of the classification results was assessed based on the test sets of ground-truth control points. Error matrices represent collated occurrences of all samples with predicted and reference membership (Foody, 2002). The following statistics were then determined: User's, Producer's, and Overall Accuracy. While the User's accuracy provides a statistic from the map user's perspective, the Producer's accuracy estimates it from the map maker's perspective. The overall accuracy provides the ratio of correctly classified samples to all test samples. To ensure readability and comparability of the results, all error matrices provided in this study were presented as percentages. Error matrices and accuracy assessment results were calculated using ArcGIS and R software.

3. Results

3.1. Feature extraction and selection

Fig. 4 represents the slope extracted from ALB, divided for the units described in the methodology section. It shows that the majority of areas are within flat, inclined and low steep areas, whereas some sandbars and coastal protection structures are characterised by steeper slope.

The other predictor variable was diagnostic for the determination of sandbar crests – the Multiresolution Index of Ridge Top Flatness (Gallant and Dowling, 2003, see Table 4). MRRTF values higher than 0.5 correspond to the steepest and smallest distinguishable ridge tops. Flatter and larger ridge tops are represented by higher values. Similarly, high values of MRRTF show good agreement with ridge tops, manually determined for selected areas (Fig. 5A-C). In addition, there is a clear boundary between low and high values in the MRRTF derivative. Thus, MRRTF is an appropriate feature for the automatic determination of the course and widths of sandbar crests and ridge tops of smaller bedforms, such as megaripples (Fig. 5).

The results of the Boruta feature selection algorithm indicate that all extracted features were relevant for classification in all scenarios. Since the Boruta algorithm creates “shadow variables” by perturbing the original features to generate a randomised version of them, the features become relevant when they exceed an importance score higher than the best randomised feature. For this reason, all supervised classifiers were trained with all features in this study.

3.2. Comparison of manual and supervised classification results

Manual classifications were conducted by a single interpreter to

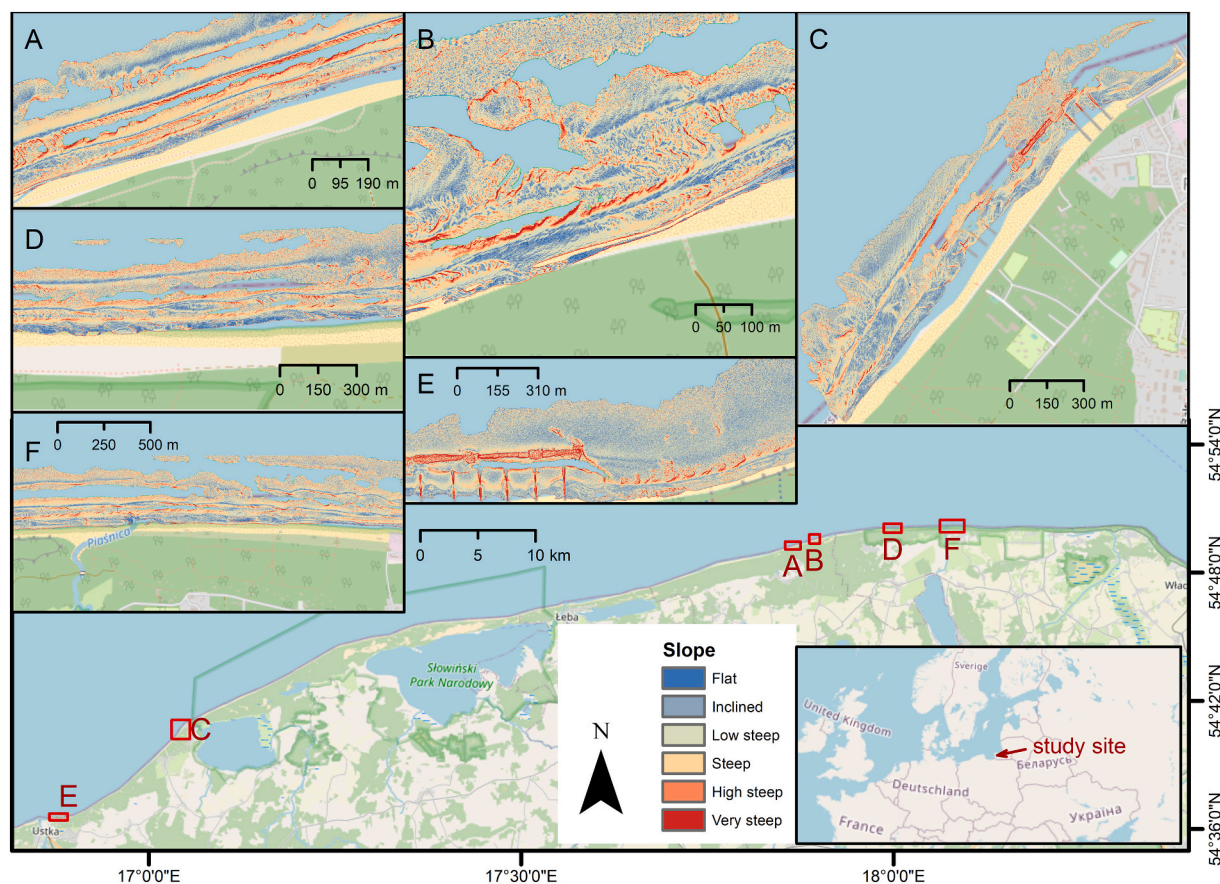


Fig. 4. Results of the slope predictor variable divided for separate units. A – study site N1; B – study site N2; C – study site A1; D – study site N3; E – study site N4; F – study site A2. Basemap: Openstreetmap.

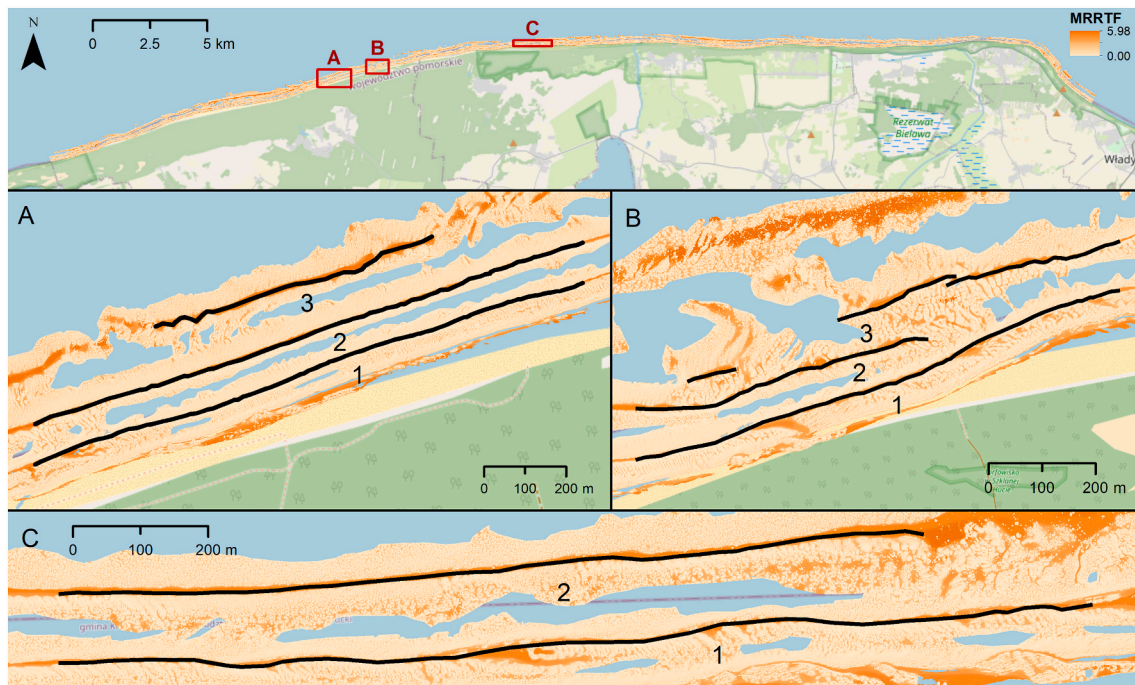


Fig. 5. Results of MRRTF predictor variable extraction for 48 km of the nearshore area of the Polish coast; A–C – subsets marked on the general map (subsets apply only to this particular figure). Black lines represent manually digitised shapes of sandbar crests (1–3). Basemap: Openstreetmap.

obtain a uniform, interpretatively consistent picture of the seafloor. Separations were introduced during one interpretation period lasting three days. Interpretation was performed on the first two days, while the uniformity and consistency of the introduced separations were checked on the third day.

Of all the supervised classifiers tested, RF had the highest performance and accuracy in all scenarios. Therefore, all maps provided below show results of the RF classification after the map generalisation described in the methods (Figs. 6–8). The automatic classification results were collated with manual determined maps on the left side of the following figures (Figs. 6–8).

Comparison of the supervised classification results for study sites N1–N4 shows good agreement for all major classes covering large areas of the study sites (Fig. 6). This is particularly evident when comparing the spatial coverage of bedform units such as undulating bed, plain bed, and ripples. There are some shortcomings in the supervised classification results, for example, in the spatial coverage of artefacts at study sites N2 and N4, but they do not distort the overall good picture of the results.

The comparison of the supervised classification results for study sites A1–A2 is presented in Fig. 7. Although both areas are similarly complex in terms of the occurrence of bedforms, the supervised classification result for area A1 was of lower quality than for area A2. The difference is not significant, the main bedforms were correctly determined, but study site A1 contains some scattered irregularities that may be remnants of the generalisation procedure or the result of data heterogeneity. Furthermore, the spatial arrangement of the areas occupied by different bedforms at study site A1 is more varied than at study site A2, where the plain bed of one class covers the vast majority of the area (57.85%). The strengths and weaknesses of the classification, as well as the classifier performance, are also reflected in the error matrices presented and explained in the next section.

The application of the supervised classification for 48 km of the Polish coast of the Southern Baltic is shown in Fig. 8. The map is the result of the second model (G2), described in the Methods section (classification trained with samples from study sites N1/N2/N4, validated with samples from study site N3). The subsets presented in Fig. 7

represent regions classified based on ground-truth control points located in other areas, demonstrating the good performance of the RF classifier. While the overall delineations of the main bedform units were correctly determined, residuals of the classification artefacts are visible. The following section describes the qualitative accuracy results for all study sites presented in this study.

3.3. Accuracy assessment

Fig. 9 provides an insight into the overall statistics for all supervised classification results obtained in this study. The results indicate that the RF classifier had the highest classification performance, while the SVM algorithm had the worst accuracy statistics for most of the study sites.

The tables in Appendix A provide detailed error matrices and accuracy assessment statistics for all areas and classifiers. Tables A1–A16 present accuracy results for study sites N1–N4, Tables A17–A24 show results for anthropogenic study sites A1–A2, A25–26 present results for two models (G1–G2) for the 48 km nearshore zone of the Polish coast. All RF results represent good to very good accuracy of the developed classification models. The overall accuracy in all scenarios ranged from more than 75% to 91%, with a median of 84%.

Study site N1 reached the highest accuracy in automatic classification (Table A4). It was high for all classes except for the Producer's accuracy for the undulating bed class (53%). The overall accuracy of the RF classification results for other natural study sites was in the range of 83–86% (Table A4; A8; A12; A16). Potential shortcomings of the RF classification per class were related, for example, to the class of undulating bed with artefacts at study site N3 (Table A12), the class of artefacts in area N4 (Table A16), and the class of straight or sinuous ripples at study site N4 (Table A16). As the study sites were divided into 7–8 classes of bedforms, the obtained results were evaluated as sufficient for a comprehensive description of the nearshore zone in the analysed areas.

The results of the RF supervised classification for anthropogenic study sites A1–A2 are presented in Table A20/A24. Area A1 was divided into 11 units, whereas study site A2 was divided into 10 classes. The overall accuracy of the RF classifier of study site A1 was the lowest of all the results presented. In comparison, the RF results for area A2 reached

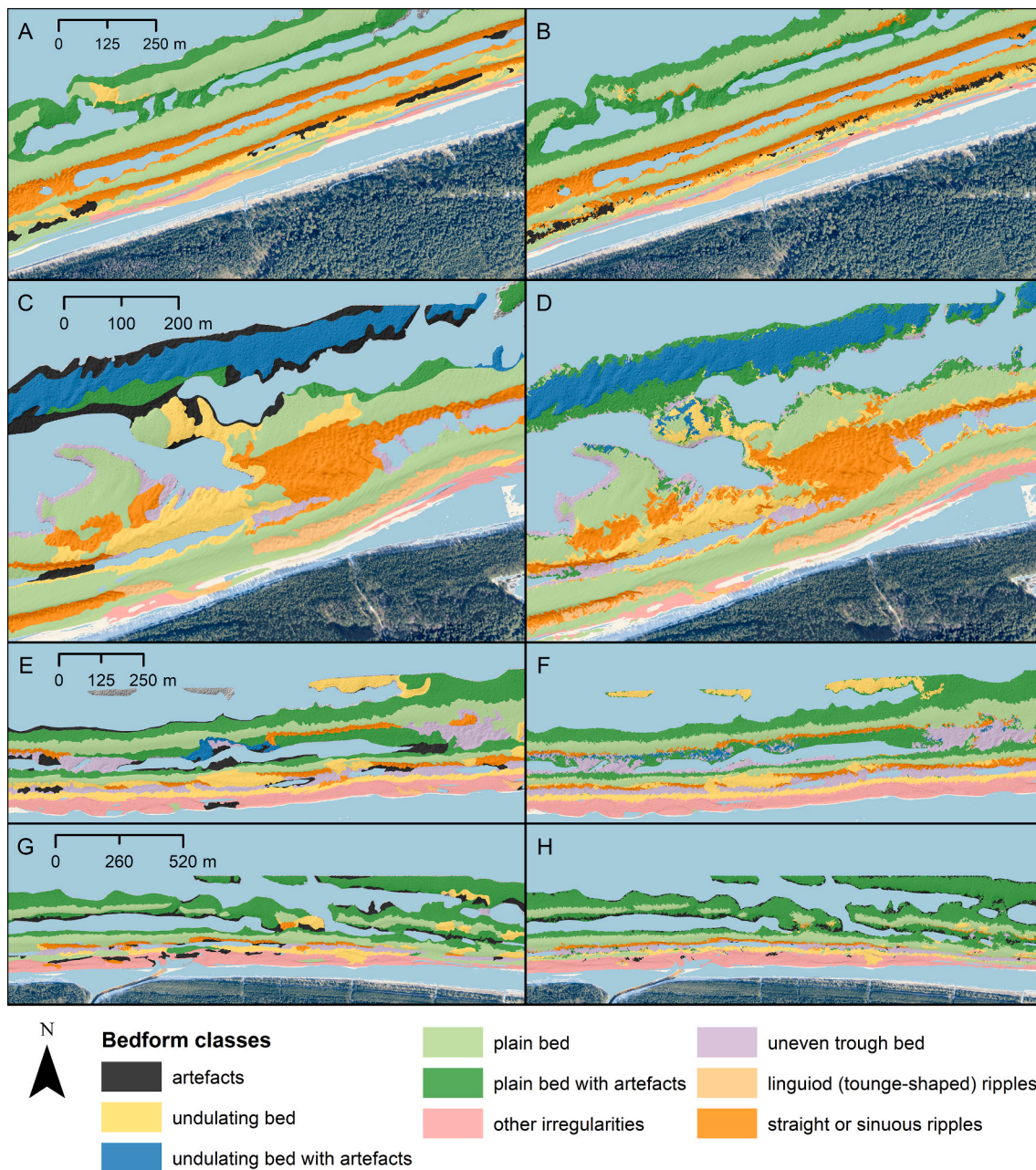


Fig. 6. Comparison of the manual (A, C, E, G) and RF supervised classification (B, D, F, H) results. Specific rows represent subsequent study sites N1–N4 (top–down). Basemap – auxiliary orthophotomap from the same aerial survey.

85% overall accuracy (Table A24). In both areas, all classes were distinguished rather properly, with some minor shortcomings. At study site A1, these include i.a. units of artefacts, other irregularities, and submerged breakwaters. In comparison, in scenario A2 they include i.a. artefacts and straight or sinuous ripples. On the other hand, given the variety of classes and complexity of the survey task, the quantitative results of both scenarios should be regarded as highly satisfactory.

As mentioned in the Methods section, the maps for the 48 km nearshore area were generated and validated based on the data set of the merged control points of study sites N1–N4. Therefore, the supervised classification results for two models G1–G2 covering the large spatial dataset can be considered statistically significant. Both models classified the area into nine units of natural bedforms and artefacts. The first model had an overall accuracy of 81%, whereas the second one reached an accuracy of 85% (Table A25; A26). Some classes were accurately determined in both models, e.g. units of the undulating bed, undulating

bed with artefacts, and uneven trough bed. In addition, both models had some shortcomings, like weak Producer's accuracy for the class of artefacts in both models, weak User's accuracy for the plain bed with artefacts/other irregularities in model G1, weak Producer's accuracy for linguoid ripples in model G2. However, a large discrepancy between the User's and Producer's accuracy can be observed (Table A25; A26). As the evaluation of the trained classifiers for a new area cannot be performed solely based on quantitative results, we compared them with visual image interpretation. In this way, we decided that model G2 showed better classification performance and generated fewer residual miscalculations. An independent expert interpretation confirmed that the resulting separations are possible and correct.

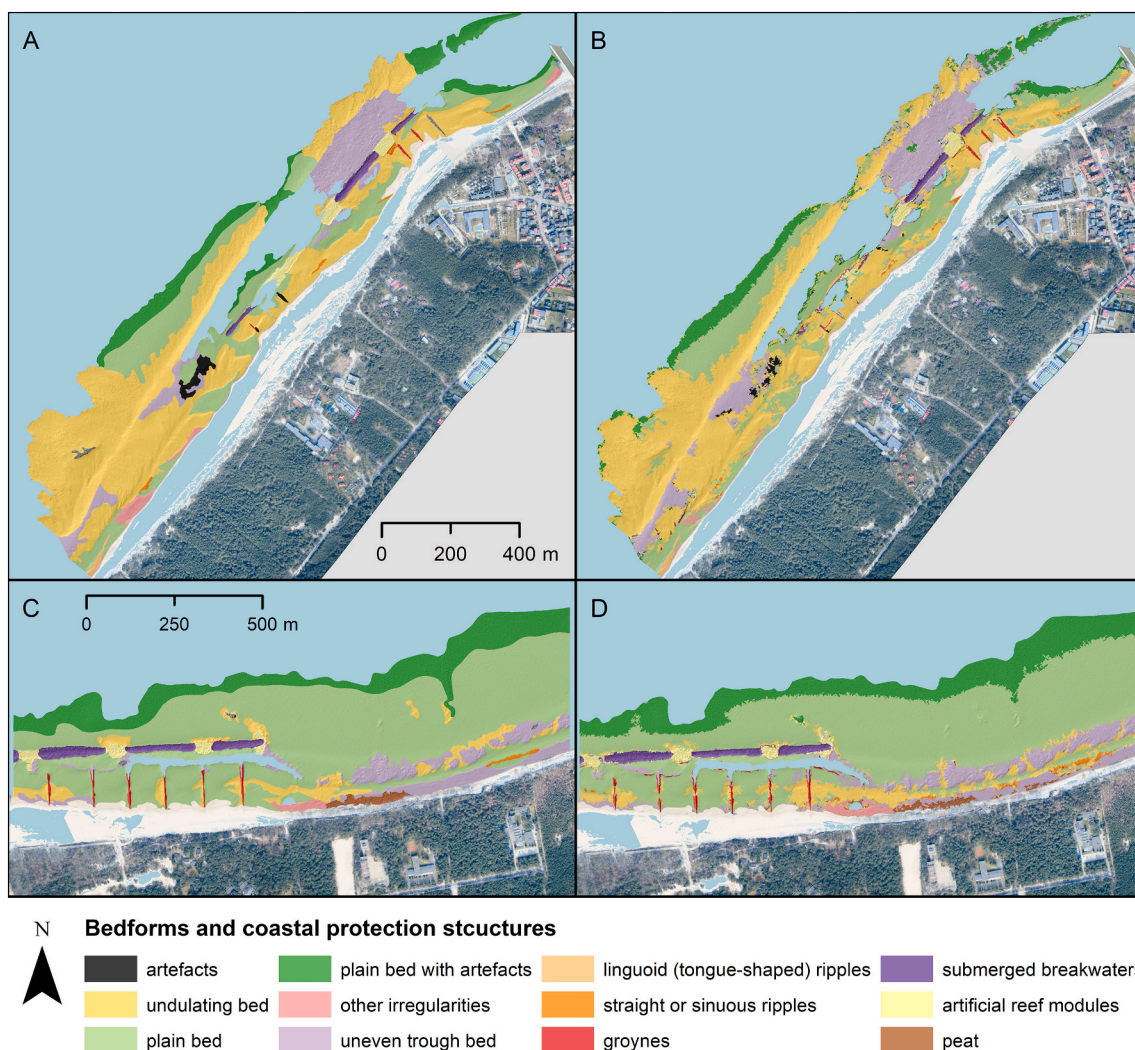


Fig. 7. Comparison of the manual (A, C) and RF supervised classification (B, D) results for study sites A1 (top) and A2 (down). Basemap – supporting orthophotomap from the same aerial survey.

4. Discussion

4.1. Relevance of the main findings of the article

This study has shown that the RF classifier is most suitable for accurate automatic classification of geomorphological bedforms and anthropogenic structures based on ALB datasets. Our study sites N1–N4, A1–A2 and models G1–G2 have demonstrated that RF can successfully handle complex classification tasks with numerous separations. In addition, the algorithm performed well on large sets of all predictor variables that were evaluated as significant after applying the Boruta feature selection algorithm.

Many other studies addressing automatic classification of underwater bedforms confirm the robustness of the RF classification algorithm (e.g., Turner et al., 2018). RF is already occasionally used as the only classifier in some underwater seafloor studies (e.g., Dolan et al., 2021). Our results suggest that RF is the most suitable algorithm for automatic mapping of bedforms based on ALB datasets.

Initially developed for hydrological purposes (Gallant and Dowling, 2003), the MRRTF was successfully applied to swiftly delineate sandbar crests in the nearshore zone of the study sites presented in this study. Although, to the best of our knowledge, the MRRTF has only been used once in underwater applications (Janowski et al., 2021), it appears to be very useful and relevant for underwater exploration of the seabed.

Possible applications include not only the determination of the course of crests but also their relative width.

The results of the automatic analyses were compared with the results of the manual analyses. Human vision aggregates similar pixels in an image into groups and distinguishes different forms and spatial relationships. However, to make these associations visible, the image must be analysed at a certain scale that allows the distinction of geomorphological forms. As mentioned in the Methods, manual interpretation was determined with a scale precision of 1:5000 or greater to capture the course of geomorphological forms. Automatic segmentation can perform the same task, attributing the texture of an area, its shape and contextual information, allowing accurate boundary delineation at a very high scale (even considering pixel to pixel boundaries). Therefore, automatic classifications may be much more detailed than their manual counterparts. In our work, the precision of separations is lower on the manual maps compared to automatic interpretation. During the manual seabed geomorphological analysis, the boundaries between individual seabed types were plotted with generalisation resulting from the scale of a map on which they were interpreted. During automatic segmentation and classification, these boundaries retain full resolution of the source data, hence their more varied course. Furthermore, the automatic interpretation maps provide greater detail by indicating study sites that were not separated during manual classification. Areas that were automatically delineated, but were not indicated during manual interpretation, were

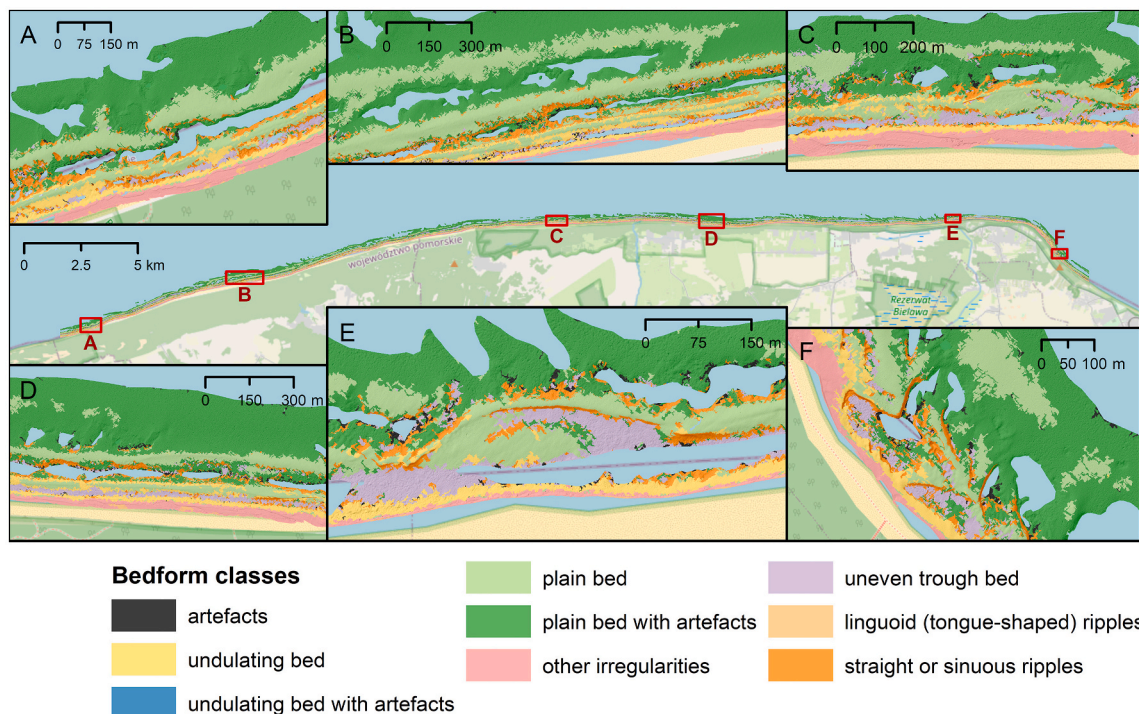


Fig. 8. Results of the RF supervised classification of model G2 for 48 km of the nearshore area of the Polish coast; A–F – subsets of the study site marked on the general map (subsets apply only to this particular figure). Basemap: Openstreetmap.

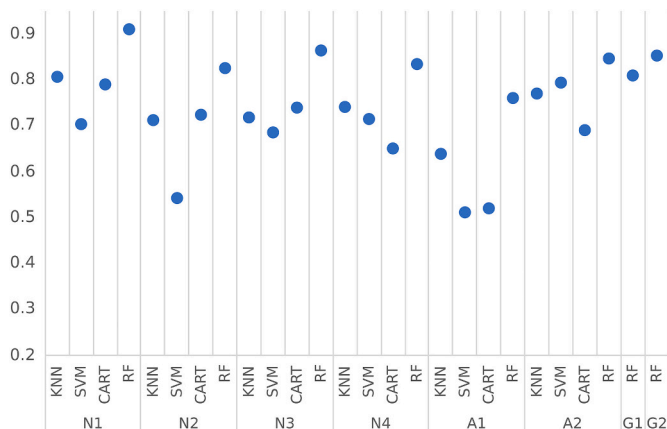


Fig. 9. Comparison of the overall accuracy statistics for all tested supervised classifiers and all study sites.

checked for the possibility of introducing such delineations into the manually interpreted maps. The analysis shows that such an interpretation is possible and correct.

Both manual and automatic interpretation involve the preparation of interpretation assumptions by author. This entails a subjective approach to separation and was not pointed out as an error. It is important to note, however, that during automatic analysis the level of subjectivity is far more “stable” than during manual interpretation. It is usually more challenging to maintain the uniformity and homogeneity of the introduced separations during manual analysis. This is due to the author’s approach to analysis and the subjective view of the analysed area, which varies depending on the interpreting person. Therefore, in our research, the study sites were interpreted by one person in a relatively short time (approximately one hour for one study site). Such problems do not exist during automated analysis. The advantage of automatic analysis is its greater interpretative homogeneity and the time required to perform the

analysis. Once generated, a single run of the GEOBIA model took several seconds, which is negligible compared to the time required for manual delineation.

The smallest differences between the manual and automatic interpretation results were in the flat and rippled areas of the seabed. The largest differences were observed within the uneven seabed. Within such sections of the seabed, general separations of the “uneven trough bed” type or “other irregularities” were more frequently introduced during the manual analysis. As a result of the automatic analysis, additional, more detailed separations were introduced in the same areas due to higher resolution of the analyses. Some of these separations, due to their small areas, were removed in accordance with the adopted minimum area of a single study site (400 m²).

4.2. Limitations of our research

The results of the accuracy assessment showed that determinations of the classes were less precise for the study sites with artefacts. For example, an undulating bed with artefacts may be interpreted in the same way as a plain bed with artefacts. Since the area occupied by artefacts can be morphometrically heterogeneous, it was difficult for the classifiers to adequately separate these units. In contrast, other bedforms with a higher quality of data measurement were clearly separated.

Moreover, without the presence of artefacts, the overall accuracy would probably be higher. In order to check how artefacts may disturb the final result of the best classifiers, we merged the class of undulating bed with the class of undulating bed with artefacts, as well as the class of plain bed with the class of plain bed with artefacts. As a result, the classifications were simplified by two types of bedforms (with artefacts). Fig. 10 shows a general comparison of the overall accuracy statistics for all study sites and the simplified classification scheme (we used the RF algorithm for all calculations). Additional detailed calculations of the error matrices provided in Tables A27–A32 give an idea of how they may affect the final classification result. While the overall accuracy statistics slightly increased (in the range of 1–3%) for almost all study sites, it surprisingly increased by +7% in the case of model G1. In

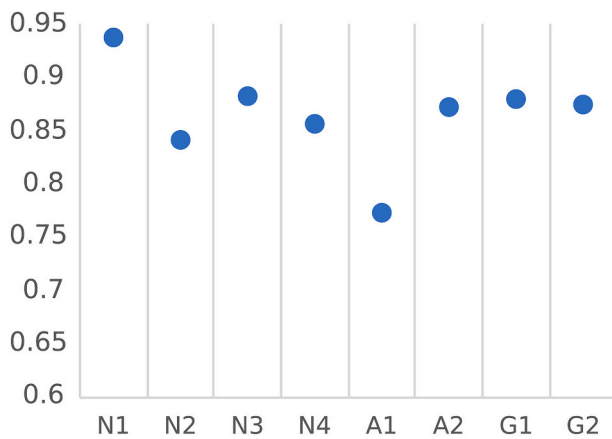


Fig. 10. Comparison of the overall accuracy statistics for all study sites and simplified bedform classes.

general, the presented analyses confirm that the quality of the input data affects the classification result. A DEM with a large number of artefacts would likely reduce the accuracy of the result.

A certain limitation (which does not result from our method, but rather limits it), is the range of the measurement method – the penetration range and the seabed data coverage. The depth at the study site ranged from 4.7 m (study site N4) to 5.5 m (study site A2). These limitations result from the water turbidity (suspended matter, algae, gas bubbles) and the capabilities of the applied measurement methods. A prerequisite for assessing the ability of LiDAR technology to penetrate the seabed forms is the depth of the Secchi disc. Experiments with LiDAR technology in the Baltic Sea showed that with the use of penetrating equipment above 1 Secchi depth, it is possible to record depths down to several meters. However, this also shows the problem of bottom sediments that do not reflect the beam. This involves the problem of efficient spending of resources on measurement research. However, by showing the results of our research, we open the way for correct interpretation of results and show the possibility of using this technology in offices dealing with coastal protection. The measurements did not cover the entire strip of the sandbar zone, but only a shallower part of this zone and the peak parts of the bars located deeper, farther from the shore. Based on these data, it is possible to conclude about the distribution of sandbars and the variability in their location. However, limitations may arise when making detailed conclusions about the dynamics, variability, and character of the sandbar zone based on the analysis of formations within the sandbars and depressions between them, as well as when analysing the directions of water movement and sediment transport. In the examples presented, a seabed data coverage of 90–95% was achieved for shallow parts of the sandbar zone (bar 1 and bar 2). For deeper parts of the seabed, the coverage was less than 70%.

The previous use of topo-bathymetric LiDAR in tidal environments showed successful classification of mainly emerged geomorphological forms (Andersen et al., 2017). Similarly, Schmidt et al. (2013) classified the LiDAR point cloud in the German North Sea for the following three classes: mudflat, water, and mussel bed. Their study shows that automatic classification, incorporating multiple secondary features, can precisely determine land-water boundaries that may vary during tides. Because the scope of this study was to classify submerged bedforms in a non-tidal environment, we did not pay attention to landforms above the sea surface. However, since topo-bathymetric LiDAR also allows the measurements of landforms, it would be interesting to test our geomorphological mapping approach above the water surface. Furthermore, Cottin et al. (2014) analysed full backscatter waveforms of bathymetric LiDAR to determine up to nine benthic habitat classes related to the seafloor substrate, such as sand, gravels or kelps. In our case, the LiDAR full-waveform dataset was not available, so our

automatic mapping was performed based on ALB and its multiple secondary features. Nevertheless, it can be assumed that if a bathymetric lidar backscatter is available, it would be possible to delineate much more detailed areas, considering local differences in sediments.

4.3. Recommendations for future research

Although this study confirmed that the RF performance was the highest of all four tested supervised classifiers, there is room to explore other (also unsupervised) classifiers, as well as a combined approach (Dolan et al., 2021; Turner et al., 2018). Furthermore, it would be worthwhile to test the RF classifier in different environments and bodies of water with other physical properties. Moreover, the segmentation algorithms underlying the GEOBIA approach include more than just multiresolution segmentation. This algorithm is the most verified and common in the literature, but there is a need for further research to evaluate multiresolution segmentation with alternatives, like semantic segmentation (Chen et al., 2018) or the RSOBIA (Remote Sensing Object Based Image Analysis) approach (Prampolini et al., 2021).

The results of the Boruta feature selection algorithm indicate that all predictor variables were relevant for the classification. Therefore, it seems reasonable to increase the number of geomorphic attributes or include variables from different sources. Possible paths of development are, for example, DEM spectral features, textural features or oceanographic variables (Dolan et al., 2021). Increasing the number of available predictor variables could result in better differentiation of their suitability for classification.

The development of a high-quality DEM is a basic requirement for the correct application of the methods presented in this article. However, the more accurate the DEM, the greater the costs of measurements. Our research has shown the suitability of ALB datasets for automatic classification of bedforms. The versatility of the presented method suggests its applicability in similar coastal sections of the southern Baltic Sea. However, due to many factors described in this article, data coverage of high-quality ALB datasets may not be satisfactory. Therefore, our future research will focus on maximising the depth coverage of aerial measurements, maintaining high-quality and minimising the costs of their implementation.

The potential assessment and design of new coastal protection structures require detailed research, including geotechnical studies. It is important to determine appropriate representative values of soil parameters, correlations, and their standard deviations. Hypotheses formulated during the research phase may be the subject of field research. The importance of the presented approach can be supported by tests described in Ossowski et al. (2019), where the change in geotechnical parameters indicated a high sensitivity of the examined cliff. Therefore, by observing the conditions that affect changes in geotechnical parameters, the determination of a degradation route will improve the safety of the region. This is important as coastal degradation is progressing due to the increasing frequency of severe weather events.

4.4. Conclusions

The research presented in this paper covers different aspects of the determination and evaluation of automatic mapping methods based on ALB datasets. Nine geomorphological bedforms and three anthropogenic structures occurring in the nearshore zone of the Southern Baltic were distinguished, proving the suitability of high-resolution ALB datasets for automatic mapping of such bedforms. The determination of the MRRTF can be successfully employed to automatic delineation of sandbar crests, which are of great importance for coastal protection. The ALB spatial coverage presented in this article shows that there is still room for improvement in the accuracy and penetration range of bathymetric LiDAR measurements. Although multiple geomorphometric predictor variables were evaluated for automatic mapping in this study, secondary features from other sources may improve classification

performance.

Author contributions

Conceptualisation, L.J., R.W., M.R., A.K-G., P.T.; methodology, L.J.; software, L.J.; validation, P.T.; formal analysis, L.J.; investigation, L.J., R.W., M.R., A.K-G.; resources, A.K-G., P.T.; data curation, L.J., R.W., M.R., A.K-G., P.T.; writing — original draft preparation, L.J., R.W., M.R., A.K-G., P.T.; writing — review and editing, L.J., R.W., M.R., A.K-G., P.T.; visualisation, L.J., P.T.; supervision, L.J.; project administration, L.J.; funding acquisition, L.J. All authors have read and agreed to the published version of the manuscript.

Funding

This research was funded in whole or in part by National Science Centre, Poland [Grant number: 2021/40/C/ST10/00240]. For the

purpose of Open Access, the authors have applied a CC-BY public copyright licence to any Author Accepted Manuscript (AAM) version arising from this submission.

Data availability statement

The data that support the findings of this study are available from the corresponding author upon reasonable request.

Declaration of Competing Interest

The authors declare that they have no known competing financial interests or personal relationships that could have appeared to influence the work reported in this paper.

The authors declare the following financial interests/personal relationships which may be considered as potential competing interests:

Appendix A. Appendix

Table A1

Error matrix and accuracy assessment statistics for the KNN supervised classifier and study site N1. Unit labels: 1 – artefacts, 2 – undulating bed, 4 – plain bed, 5 – plain bed with artefacts, 6 – other irregularities, 8 – linguoid (tongue-shaped) ripples, 9 – straight or sinuous ripples. Pred\Ref – Prediction\Reference.

Pred\Ref	1	2	4	5	6	8	9	Sum
1	1.20	0.20	0.00	0.13	0.00	0.00	0.27	1.80
2	0.00	2.40	1.54	0.40	0.00	0.07	1.34	5.74
4	0.20	1.00	49.43	2.87	0.20	0.13	2.54	56.38
5	0.13	0.53	2.20	12.42	0.00	0.07	1.07	16.43
6	0.00	0.00	0.13	0.00	1.54	0.13	0.00	1.80
8	0.07	0.07	0.00	0.00	0.33	1.34	0.00	1.80
9	0.40	1.34	1.47	0.53	0.00	0.00	12.29	16.03
Sum	2.00	5.54	54.78	16.37	2.07	1.74	17.50	100.00
User's	0.6667	0.4186	0.8768	0.7561	0.8519	0.7407	0.7667	
Producer's	0.6000	0.4337	0.9024	0.7592	0.7419	0.7692	0.7023	
Overall	0.8063							

Table A2

Error matrix and accuracy assessment statistics for the SVM supervised classifier and study site N1. Unit labels: 1 – artefacts, 2 – undulating bed, 4 – plain bed, 5 – plain bed with artefacts, 6 – other irregularities, 8 – linguoid (tongue-shaped) ripples, 9 – straight or sinuous ripples. Pred\Ref – Prediction\Reference.

Pred\Ref	1	2	4	5	6	8	9	Sum
1	1.07	0.07	0.07	0.00	0.00	0.00	0.20	1.40
2	0.20	0.94	1.34	0.00	0.00	0.00	1.80	4.28
4	0.27	2.00	42.95	4.01	0.00	0.13	4.34	53.71
5	0.00	0.60	2.00	12.29	0.00	0.00	1.20	16.10
6	0.00	0.33	0.20	0.00	1.74	0.20	0.00	2.47
8	0.00	0.00	0.00	0.00	0.33	1.40	0.00	1.74
9	0.47	1.60	8.22	0.07	0.00	0.00	9.95	20.31
Sum	2.00	5.54	54.78	16.37	2.07	1.74	17.50	100.00
User's	0.7619	0.2188	0.7998	0.7635	0.7027	0.8077	0.4901	
Producer's	0.5333	0.1687	0.7841	0.7510	0.8387	0.8077	0.5687	
Overall	0.7034							

Table A3

Error matrix and accuracy assessment statistics for the CART supervised classifier and study site N1. Unit labels: 1 – artefacts, 2 – undulating bed, 4 – plain bed, 5 – plain bed with artefacts, 6 – other irregularities, 8 – linguoid (tongue-shaped) ripples, 9 – straight or sinuous ripples. Pred\Ref – Prediction\Reference.

Pred\Ref	1	2	4	5	6	8	9	Sum
1	1.54	0.60	0.94	0.00	0.00	0.00	1.60	4.68
2	0.13	2.94	5.81	0.40	0.00	0.00	1.00	10.29
4	0.00	0.40	42.82	0.33	0.00	0.00	1.27	44.82
5	0.00	0.27	3.41	15.16	0.00	0.00	0.07	18.90
6	0.00	0.53	0.33	0.00	1.60	0.33	0.00	2.81
8	0.00	0.00	0.20	0.00	0.47	1.40	0.00	2.07
9	0.33	0.80	1.27	0.47	0.00	0.00	13.56	16.43

(continued on next page)

Table A3 (continued)

Pred\Ref	1	2	4	5	6	8	9	Sum
Sum	2.00	5.54	54.78	16.37	2.07	1.74	17.50	100.00
User's	0.3286	0.2857	0.9553	0.8021	0.5714	0.6774	0.8252	
Producer's	0.7667	0.5301	0.7817	0.9265	0.7742	0.8077	0.7748	
Overall	0.7902							

Table A4

Error matrix and accuracy assessment statistics for the RF supervised classifier and study site N1. Unit labels: 1 – artefacts, 2 – undulating bed, 4 – plain bed, 5 – plain bed with artefacts, 6 – other irregularities, 8 – linguoid (tongue-shaped) ripples, 9 – straight or sinuous ripples. Pred\Ref – Prediction\Reference.

Pred\Ref	1	2	4	5	6	8	9	Sum
1	1.59	0.20	0.07	0.00	0.00	0.00	0.13	1.98
2	0.07	3.04	0.33	0.00	0.00	0.07	0.40	3.90
4	0.13	0.93	51.12	0.66	0.07	0.00	0.53	53.44
5	0.00	0.53	2.12	15.41	0.00	0.00	0.00	18.06
6	0.00	0.26	0.20	0.00	1.85	0.07	0.00	2.38
8	0.00	0.07	0.00	0.00	0.20	1.59	0.00	1.85
9	0.40	0.73	0.60	0.26	0.00	0.00	16.40	18.39
Sum	2.18	5.75	54.43	16.34	2.12	1.72	17.46	100.00
User's	0.8000	0.7797	0.9567	0.8535	0.7778	0.8571	0.8921	
Producer's	0.7273	0.5287	0.9392	0.9433	0.8750	0.9231	0.9394	
Overall	0.9101							

Table A5

Error matrix and accuracy assessment statistics for the KNN supervised classifier and study site N2. Unit labels: 2 – undulating bed, 3 – undulating bed with artefacts, 4 – plain bed, 5 – plain bed with artefacts, 6 – other irregularities, 7 – uneven trough bed, 8 – linguoid (tongue-shaped) ripples, 9 – straight or sinuous ripples. Pred\Ref – Prediction\Reference.

Pred\Ref	2	3	4	5	6	7	8	9	Sum
2	5.71	0.58	1.66	0.07	0.07	0.43	0.07	1.806	10.40
3	0.51	13.44	0.65	0.94	0.00	0.00	0.07	0	15.61
4	2.67	0.72	31.94	1.01	0.65	0.58	0.65	2.673	40.90
5	0.36	1.08	0.79	2.10	0.00	0.36	0.00	0.072	4.77
6	0.00	0.07	0.29	0.00	1.16	0.00	0.07	0	1.59
7	0.14	0.14	0.51	0.29	0.00	1.08	0.00	0.217	2.38
8	0.07	0.00	0.87	0.00	0.07	0.00	3.40	0.867	5.27
9	2.31	0.14	2.89	0.43	0.00	0.07	0.79	12.43	19.08
Sum	11.78	16.18	39.60	4.84	1.95	2.53	5.06	18.06	100.00
User's	0.5486	0.8611	0.7809	0.4394	0.7273	0.4545	0.6438	0.6515	
Producer's	0.4847	0.8304	0.8066	0.4328	0.5926	0.4286	0.6714	0.6880	
Overall	0.7124								

Table A6

Error matrix and accuracy assessment statistics for the supervised classifier SVM and study site N2. Unit labels: 2 – undulating bed, 3 – undulating bed with artefacts, 4 – plain bed, 5 – plain bed with artefacts, 6 – other irregularities, 7 – uneven trough bed, 8 – linguoid (tongue-shaped) ripples, 9 – straight or sinuous ripples. Pred\Ref – Prediction\Reference.

Pred\Ref	2	3	4	5	6	7	8	9	Sum
2	1.66	0.07	2.02	0.36	0.00	0.29	0.07	3.757	8.24
3	0.87	14.96	1.23	1.88	0.00	0.14	0.00	0	19.08
4	4.70	0.36	23.84	0.94	0.00	0.29	1.81	7.298	39.23
5	0.00	0.79	0.22	0.87	0.00	0.00	0.00	0	1.88
6	0.00	0.00	3.54	0.00	1.95	0.00	0.07	0	5.56
7	0.51	0.00	0.58	0.79	0.00	1.66	0.00	0.145	3.68
8	0.00	0.00	0.22	0.00	0.00	0.00	2.75	0.289	3.25
9	4.05	0.00	7.95	0.00	0.00	0.14	0.36	6.58	19.08
Sum	11.78	16.18	39.60	4.84	1.95	2.53	5.06	18.06	100.00
User's	0.2018	0.7841	0.6077	0.4615	0.3506	0.4510	0.8444	0.3447	
Producer's	0.1411	0.9241	0.6022	0.1791	1.0000	0.6571	0.5429	0.3640	
Overall	0.5426								

Table A7

Error matrix and accuracy assessment statistics for the CART supervised classifier and study site N2. Unit labels: 2 – undulating bed, 3 – undulating bed with artefacts, 4 – plain bed, 5 – plain bed with artefacts, 6 – other irregularities, 7 – uneven trough bed, 8 – linguoid (tongue-shaped) ripples, 9 – straight or sinuous ripples. Pred\Ref – Prediction\Reference.

Pred\Ref	2	3	4	5	6	7	8	9	Sum
2	6.00	0.43	3.47	0.36	0.00	0.07	0.00	0.578	10.91
3	0.36	13.29	1.16	0.36	0.00	0.00	0.00	0	15.17
4	0.79	0.36	26.81	0.22	0.00	0.00	0.43	1.012	29.62
5	0.51	2.10	1.45	3.83	0.00	0.65	0.00	0	8.53
6	0.00	0.00	0.51	0.00	1.95	0.00	0.07	0	2.53
7	0.79	0.00	0.29	0.00	0.00	1.66	0.00	0.506	3.25
8	0.07	0.00	2.10	0.00	0.00	0.00	4.55	1.662	8.38
9	3.25	0.00	3.83	0.07	0.00	0.14	0.00	14.31	21.60
Sum	11.78	16.18	39.60	4.84	1.95	2.53	5.06	18.06	100.00
User's	0.5497	0.8762	0.9049	0.4492	0.7714	0.5111	0.5431	0.6622	
Producer's	0.5092	0.8214	0.6770	0.7910	1.0000	0.6571	0.9000	0.7920	
Overall	0.7240								

Table A8

Error matrix and accuracy assessment statistics for the RF supervised classifier and study site N2. Unit labels: 2 – undulating bed, 3 – undulating bed with artefacts, 4 – plain bed, 5 – plain bed with artefacts, 6 – other irregularities, 7 – uneven trough bed, 8 – linguoid (tongue-shaped) ripples, 9 – straight or sinuous ripples. Pred\Ref – Prediction\Reference.

Pred\Ref	2	3	4	5	6	7	8	9	Sum
2	7.85	0.07	1.40	0.14	0.00	0.14	0.00	1.05	10.65172
3	0.56	14.79	0.35	0.91	0.00	0.07	0.00	0.00	16.67835
4	1.47	0.07	33.57	0.35	0.00	0.07	0.49	0.91	36.93062
5	0.21	0.98	0.63	3.29	0.00	0.28	0.00	0.00	5.395936
6	0.00	0.00	0.42	0.00	1.89	0.00	0.07	0.00	2.382621
7	0.42	0.07	0.42	0.14	0.00	1.75	0.00	0.14	2.943238
8	0.00	0.00	0.98	0.00	0.00	0.00	4.48	1.05	6.517169
9	1.89	0.00	1.33	0.07	0.00	0.14	0.14	14.93	18.50035
Sum	12.4	15.98	39.1	4.905	1.892	2.453	5.186	18.08	100
User's	0.7368	0.8866	0.9089	0.6104	0.7941	0.5952	0.6882	0.807	
Producer's	0.6328	0.9254	0.8584	0.6714	1.0000	0.7143	0.8649	0.826	
Overall	0.8255								

Table A9

Error matrix and accuracy assessment statistics for the KNN supervised classifier and study site N3. Unit labels: 2 – undulating bed, 3 – undulating bed with artefacts, 4 – plain bed, 5 – plain bed with artefacts, 6 – other irregularities, 7 – uneven trough bed, 8 – linguoid (tongue-shaped) ripples, 9 – straight or sinuous ripples. Pred\Ref – Prediction\Reference.

Pred\Ref	2	3	4	5	6	7	8	9	Sum
2	8.68	0.00	1.18	1.46	0.69	0.90	0.00	1.528	14.44
3	0.00	0.21	0.00	0.56	0.00	0.49	0.00	0	1.25
4	0.83	0.07	18.82	2.78	0.42	0.63	0.07	0.069	23.68
5	2.36	0.56	1.04	23.68	0.14	2.64	0.00	1.319	31.74
6	0.63	0.00	0.14	0.00	13.19	0.00	0.14	0	14.10
7	0.63	0.35	0.35	2.01	0.00	5.97	0.00	0.486	9.79
8	0.00	0.00	0.00	0.00	0.14	0.00	0.21	0	0.35
9	1.18	0.07	0.35	1.32	0.00	0.69	0.00	1.04	4.65
Sum	14.31	1.25	21.88	31.81	14.58	11.32	0.42	4.44	100.00
User's	0.6010	0.1667	0.7947	0.7462	0.9360	0.6099	0.6000	0.2239	
Producer's	0.6068	0.1667	0.8603	0.7445	0.9048	0.5276	0.5000	0.2344	
Overall	0.7181								

Table A10

Error matrix and accuracy assessment statistics for the SVM supervised classifier and study site N3. Unit labels: 2 – undulating bed, 3 – undulating bed with artefacts, 4 – plain bed, 5 – plain bed with artefacts, 6 – other irregularities, 7 – uneven trough bed, 8 – linguoid (tongue-shaped) ripples, 9 – straight or sinuous ripples. Pred\Ref – Prediction\Reference.

Pred\Ref	2	3	4	5	6	7	8	9	Sum
----------	---	---	---	---	---	---	---	---	-----

(continued on next page)

Table A10 (continued)

Pred\Ref	2	3	4	5	6	7	8	9	Sum
2	7.78	0.21	1.39	2.01	0.07	0.69	0.00	1.528	13.68
3	0.00	0.00	0.00	0.00	0.00	0.00	0.00	0	0.00
4	1.74	0.00	15.63	2.78	0.14	0.35	0.00	0.139	20.76
5	3.26	0.97	4.79	26.67	0.00	6.18	0.00	2.083	43.96
6	0.63	0.00	0.00	0.00	14.38	0.00	0.42	0	15.42
7	0.83	0.07	0.07	0.35	0.00	4.03	0.00	0.625	5.97
8	0.00	0.00	0.00	0.00	0.00	0.00	0.00	0	0.00
9	0.07	0.00	0.00	0.00	0.00	0.07	0.00	0.07	0.21
Sum	14.31	1.25	21.88	31.81	14.58	11.32	0.42	4.44	100.00
User's	0.5685	0.0000	0.7525	0.6066	0.9324	0.6744	0.0000	0.3333	
Producer's	0.5437	0.0000	0.7143	0.8384	0.9857	0.3558	0.0000	0.0156	
Overall	0.6854								

Table A11

Error matrix and accuracy assessment statistics for the CART supervised classifier and study site N3. Unit labels: 2 – undulating bed, 3 – undulating bed with artefacts, 4 – plain bed, 5 – plain bed with artefacts, 6 – other irregularities, 7 – uneven trough bed, 8 – linguoid (tongue-shaped) ripples, 9 – straight or sinuous ripples. Pred\Ref – Prediction\Reference.

Pred\Ref	2	3	4	5	6	7	8	9	Sum
2	10.28	0.00	1.32	3.33	0.28	0.76	0.00	0.278	16.25
3	0.07	0.63	0.14	2.85	0.00	1.39	0.00	0.208	5.28
4	0.56	0.00	16.74	0.49	0.00	0.35	0.00	0.069	18.19
5	0.35	0.07	1.67	22.36	0.00	0.69	0.00	0.139	25.28
6	0.97	0.00	0.07	0.00	13.54	0.00	0.14	0	14.72
7	0.49	0.21	0.42	2.01	0.00	6.81	0.00	0.417	10.35
8	0.00	0.00	0.00	0.00	0.76	0.00	0.28	0	1.04
9	1.60	0.35	1.53	0.76	0.00	1.32	0.00	3.33	8.89
Sum	14.31	1.25	21.88	31.81	14.58	11.32	0.42	4.44	100.00
User's	0.6325	0.1184	0.9198	0.8846	0.9198	0.6577	0.2667	0.3750	
Producer's	0.7184	0.5000	0.7651	0.7031	0.9286	0.6012	0.6667	0.7500	
Overall	0.7396								

Table A12

Error matrix and accuracy assessment statistics for the RF supervised classifier and study site N3. Unit labels: 2 – undulating bed, 3 – undulating bed with artefacts, 4 – plain bed, 5 – plain bed with artefacts, 6 – other irregularities, 7 – uneven trough bed, 8 – linguoid (tongue-shaped) ripples, 9 – straight or sinuous ripples. Pred\Ref – Prediction\Reference.

Pred\Ref	2	3	4	5	6	7	8	9	Sum
2	10.52	0.00	0.34	0.27	0.13	0.20	0.00	0.20	10.65
3	0.00	0.47	0.00	0.94	0.00	0.27	0.00	0.07	16.68
4	1.08	0.07	19.55	0.88	0.00	0.47	0.00	0.13	36.93
5	0.54	0.07	1.01	28.19	0.00	0.61	0.00	0.13	5.40
6	0.20	0.00	0.07	0.00	14.03	0.00	0.40	0.00	2.38
7	0.54	0.27	0.54	1.42	0.00	9.98	0.00	0.40	2.94
8	0.00	0.00	0.00	0.00	0.00	0.00	0.13	0.00	6.52
9	1.21	0.47	0.20	0.13	0.00	0.34	0.00	3.51	18.50
Sum	12.4	15.98	39.1	4.905	1.892	2.453	5.186	18.08	100.00
User's	0.9876	0.0283	0.5295	5.2236	5.8866	3.3907	0.0207	0.1895	
Producer's	0.8481	0.0295	0.5001	5.7459	7.4128	4.0689	0.0260	0.1939	
Overall	0.8638								

Table A13

Error matrix and accuracy assessment statistics for the KNN supervised classifier and study site N4. Unit labels: 1 – artefacts, 2 – undulating bed, 4 – plain bed, 5 – plain bed with artefacts, 6 – other irregularities, 7 – uneven trough bed, 9 – straight or sinuous ripples. Pred\Ref – Prediction\Reference.

Pred\Ref	1	2	4	5	6	7	9	Sum
1	2.40	0.27	0.00	2.13	0.27	0.20	0.07	5.33
2	0.13	3.20	1.73	1.07	0.53	0.07	0.27	7.00
4	0.07	1.93	17.80	2.93	0.73	0.13	0.40	24.00
5	1.93	1.40	2.60	36.00	0.13	0.87	0.40	43.33
6	0.40	0.73	1.00	0.00	12.00	0.07	0.27	14.47
7	0.47	0.20	0.13	0.27	0.07	1.80	0.20	3.13
9	0.07	0.13	0.73	0.47	0.13	0.33	0.87	2.73
Sum	5.47	7.87	24.00	42.87	13.87	3.47	2.47	100.00
User's	0.4500	0.4571	0.7417	0.8308	0.8295	0.5745	0.3171	

(continued on next page)

Table A13 (continued)

Pred\Ref	1	2	4	5	6	7	9	Sum
Producer's	0.4390	0.4068	0.7417	0.8398	0.8654	0.5192	0.3514	
Overall	0.7407							

Table A14

Error matrix and accuracy assessment statistics for the SVM supervised classifier and study site N4. Unit labels: 1 – artefacts, 2 – undulating bed, 4 – plain bed, 5 – plain bed with artefacts, 6 – other irregularities, 7 – uneven trough bed, 9 – straight or sinuous ripples. Pred\Ref – Prediction\Reference.

Pred\Ref	1	2	4	5	6	7	9	Sum
1	1.20	0.00	0.20	2.87	0.00	0.20	0.13	4.60
2	0.00	1.40	1.13	0.07	0.27	0.07	0.27	3.20
4	0.07	3.87	18.00	4.80	0.20	0.20	0.40	27.53
5	3.00	1.60	3.80	34.80	0.00	0.27	0.93	44.40
6	0.87	0.53	0.60	0.00	13.40	0.07	0.33	15.80
7	0.27	0.00	0.27	0.27	0.00	2.60	0.33	3.73
9	0.07	0.47	0.00	0.07	0.00	0.07	0.07	0.73
Sum	5.47	7.87	24.00	42.87	13.87	3.47	2.47	100.00
User's	0.2609	0.4375	0.6538	0.7838	0.8481	0.6964	0.0909	
Producer's	0.2195	0.1780	0.7500	0.8118	0.9663	0.7500	0.0270	
Overall	0.7147							

Table A15

Error matrix and accuracy assessment statistics for the CART supervised classifier and study site N4. Unit labels: 1 – artefacts, 2 – undulating bed, 4 – plain bed, 5 – plain bed with artefacts, 6 – other irregularities, 7 – uneven trough bed, 9 – straight or sinuous ripples. Pred\Ref – Prediction\Reference.

Pred\Ref	1	2	4	5	6	7	9	Sum
1	4.13	0.20	0.20	8.73	1.13	0.27	0.07	14.73
2	0.00	3.67	2.67	1.40	0.47	0.13	0.20	8.53
4	0.00	1.07	14.67	1.00	0.13	0.00	0.00	16.87
5	0.73	0.67	2.00	26.47	0.00	0.20	0.07	30.13
6	0.47	0.60	0.73	0.53	12.07	0.00	0.27	14.67
7	0.00	0.13	0.33	0.87	0.00	2.60	0.40	4.33
9	0.13	1.53	3.40	3.87	0.07	0.27	1.47	10.73
Sum	5.47	7.87	24.00	42.87	13.87	3.47	2.47	100.00
User's	0.2805	0.4297	0.8696	0.8783	0.8227	0.6000	0.1366	
Producer's	0.7561	0.4661	0.6111	0.6174	0.8702	0.7500	0.5946	
Overall	0.6507							

Table A16

Error matrix and accuracy assessment statistics for the RF supervised classifier and study site N4. Unit labels: 1 – artefacts, 2 – undulating bed, 4 – plain bed, 5 – plain bed with artefacts, 6 – other irregularities, 7 – uneven trough bed, 9 – straight or sinuous ripples. Pred\Ref – Prediction\Reference.

Pred\Ref	1	2	4	5	6	7	9	Sum
1	2.93	0.00	0.07	1.96	0.20	0.07	0.00	5.22
2	0.00	4.56	0.91	0.33	0.26	0.00	0.07	6.13
4	0.00	1.69	19.82	0.98	0.07	0.00	0.26	22.82
5	1.89	1.24	1.24	38.85	0.00	0.59	0.07	43.87
6	0.72	0.46	0.46	0.00	13.17	0.00	0.46	15.25
7	0.07	0.07	0.39	0.26	0.13	2.74	0.26	3.91
9	0.07	0.20	0.85	0.26	0.00	0.07	1.37	2.80
Sum	5.67	8.21	23.73	42.63	13.82	3.46	2.48	100.00
User's	0.5625	0.7447	0.8686	0.8856	0.8632	0.7000	0.4884	
Producer's	0.5172	0.5556	0.8352	0.9113	0.9528	0.7925	0.5526	
Overall	0.8344							

Table A17

Error matrix and accuracy assessment statistics for the KNN supervised classifier and study site A1. Unit labels: 1 – artefacts, 2 – undulating bed, 4 – plain bed, 5 – plain bed with artefacts, 6 – other irregularities, 7 – uneven trough bed, 8 – linguoid (tongue-shaped) ripples, 9 – straight or sinuous ripples, 10 – groynes, 11 – submerged breakwaters, 12 – artificial reef modules, 13 – peat. Pred\Ref – Prediction\Reference.

Pred\Ref	1	2	4	5	6	7	8	9	10	11	12	Sum
----------	---	---	---	---	---	---	---	---	----	----	----	-----

(continued on next page)

Table A17 (continued)

Pred\Ref	1	2	4	5	6	7	8	9	10	11	12	Sum
1	0.39	0.20	0.07	0.07	0.00	0.20	0.00	0.00	0.00	0.00	0.00	0.91
2	0.33	39.69	6.53	2.94	0.52	3.20	0.13	0.33	0.00	0.26	0.26	54.18
4	0.07	6.98	12.14	1.57	0.13	0.78	0.00	0.26	0.07	0.07	0.20	22.26
5	0.00	1.83	1.24	3.46	0.07	0.46	0.07	0.00	0.00	0.07	0.00	7.18
6	0.00	0.46	0.13	0.00	0.39	0.00	0.07	0.00	0.00	0.00	0.00	1.04
7	0.07	2.28	0.65	0.91	0.00	5.03	0.00	0.00	0.07	0.07	0.39	9.46
8	0.00	0.13	0.00	0.00	0.00	0.00	0.72	0.13	0.00	0.00	0.00	0.98
9	0.00	0.20	0.13	0.07	0.07	0.00	0.00	0.26	0.00	0.00	0.00	0.72
10	0.00	0.00	0.00	0.07	0.00	0.00	0.00	0.00	0.85	0.00	0.00	0.91
11	0.00	0.07	0.00	0.00	0.07	0.00	0.00	0.00	0.00	0.65	0.26	1.04
12	0.13	0.07	0.07	0.20	0.00	0.39	0.00	0.00	0.00	0.13	0.33	1.31
Sum	0.98	51.89	20.95	9.27	1.24	10.05	0.98	0.98	0.98	1.24	1.44	100.00
User's	0.4286	0.7325	0.5455	0.4818	0.3750	0.5310	0.7333	0.3636	0.9286	0.6250	0.2500	
Producer's	0.4000	0.7648	0.5794	0.3732	0.3158	0.5000	0.7333	0.2667	0.8667	0.5263	0.2273	
Overall	0.6390											

Table A18

Error matrix and accuracy assessment statistics for the SVM supervised classifier and study site A1. Unit labels: 1 – artefacts, 2 – undulating bed, 4 – plain bed, 5 – plain bed with artefacts, 6 – other irregularities, 7 – uneven trough bed, 8 – linguoid (tongue-shaped) ripples, 9 – straight or sinuous ripples, 10 – groyne, 11 – submerged breakwaters, 12 – artificial reef modules, 13 – peat. Pred\Ref – Prediction\Reference.

Pred\Ref	1	2	4	5	6	7	8	9	10	11	12	Sum
1	0.33	0.07	0.07	0.00	0.00	0.07	0.00	0.00	0.00	0.00	0.00	0.52
2	0.39	36.10	11.29	5.16	0.91	4.77	0.13	0.52	0.00	0.46	0.78	60.51
4	0.20	13.25	8.55	2.48	0.26	1.63	0.13	0.39	0.00	0.07	0.00	26.96
5	0.00	0.78	0.59	0.46	0.00	0.13	0.00	0.00	0.00	0.00	0.07	2.02
6	0.00	0.07	0.00	0.00	0.00	0.00	0.00	0.00	0.00	0.00	0.00	0.07
7	0.07	1.24	0.20	1.04	0.00	3.33	0.00	0.00	0.07	0.07	0.07	6.07
8	0.00	0.07	0.13	0.00	0.00	0.00	0.72	0.07	0.00	0.00	0.00	0.98
9	0.00	0.07	0.13	0.00	0.00	0.00	0.00	0.00	0.00	0.00	0.00	0.20
10	0.00	0.07	0.00	0.00	0.00	0.00	0.00	0.00	0.85	0.07	0.07	1.04
11	0.00	0.07	0.00	0.13	0.07	0.00	0.00	0.00	0.07	0.59	0.20	1.11
12	0.00	0.13	0.00	0.00	0.00	0.13	0.00	0.00	0.00	0.00	0.26	0.52
Sum	0.98	51.89	20.95	9.27	1.24	10.05	0.98	0.98	0.98	1.24	1.44	100.00
User's	0.6250	0.5965	0.3172	0.2258	0.0000	0.5484	0.7333	0.0000	0.8125	0.5294	0.5000	
Producer's	0.3333	0.6956	0.4081	0.0493	0.0000	0.3312	0.7333	0.0000	0.8667	0.4737	0.1818	
Overall	0.5117											

Table A19

Error matrix and accuracy assessment statistics for the CART supervised classifier and study site A1. Unit labels: 1 – artefacts, 2 – undulating bed, 4 – plain bed, 5 – plain bed with artefacts, 6 – other irregularities, 7 – uneven trough bed, 8 – linguoid (tongue-shaped) ripples, 9 – straight or sinuous ripples, 10 – groyne, 11 – submerged breakwaters, 12 – artificial reef modules, 13 – peat. Pred\Ref – Prediction\Reference.

Pred\Ref	1	2	4	5	6	7	8	9	10	11	12	Sum
1	0.52	3.52	1.17	0.26	0.07	0.72	0.00	0.00	0.07	0.00	0.07	6.40
2	0.13	22.98	1.70	0.91	0.00	0.65	0.00	0.00	0.00	0.00	0.00	26.37
4	0.00	6.14	11.29	0.39	0.00	0.13	0.00	0.07	0.00	0.07	0.13	18.21
5	0.20	5.81	1.17	5.74	0.00	0.85	0.00	0.00	0.00	0.07	0.07	13.90
6	0.00	2.28	1.89	0.00	0.85	0.00	0.07	0.00	0.00	0.00	0.00	5.09
7	0.07	5.03	0.78	1.37	0.00	6.66	0.00	0.00	0.00	0.07	0.00	13.97
8	0.00	0.59	0.52	0.00	0.00	0.00	0.85	0.07	0.00	0.00	0.00	2.02
9	0.07	2.81	1.83	0.20	0.20	0.00	0.07	0.85	0.26	0.07	0.20	6.53
10	0.00	0.20	0.00	0.00	0.00	0.00	0.00	0.00	0.65	0.20	0.07	1.11
11	0.00	1.76	0.59	0.13	0.13	0.20	0.00	0.00	0.00	0.78	0.07	3.66
12	0.00	0.78	0.00	0.26	0.00	0.85	0.00	0.00	0.00	0.00	0.85	2.74
Sum	0.98	51.89	20.95	9.27	1.24	10.05	0.98	0.98	0.98	1.24	1.44	100.00
User's	0.0816	0.8713	0.6201	0.4131	0.1667	0.4766	0.4194	0.1300	0.5882	0.2143	0.3095	
Producer's	0.5333	0.4428	0.5389	0.6197	0.6842	0.6623	0.8667	0.8667	0.6667	0.6316	0.5909	
Overall	0.5202											

Table A20

Error matrix and accuracy assessment statistics for the RF supervised classifier and study site A1. Unit labels: 1 – artefacts, 2 – undulating bed, 4 – plain bed, 5 – plain bed with artefacts, 6 – other irregularities, 7 – uneven trough bed, 8 – linguoid (tongue-shaped) ripples, 9 – straight or sinuous ripples, 10 – groyne, 11 – submerged breakwaters, 12 – artificial reef modules, 13 – peat. Pred\Ref – Prediction\Reference.

Pred\Ref	1	2	4	5	6	7	8	9	10	11	12	Sum
1	0.37	0.18	0.00	0.00	0.00	0.06	0.00	0.00	0.00	0.00	0.00	0.61
2	0.43	40.67	4.10	1.41	0.24	0.92	0.06	0.12	0.12	0.18	0.06	48.32
4	0.06	4.77	15.47	0.73	0.49	0.12	0.06	0.12	0.00	0.06	0.18	22.08
5	0.06	1.28	0.55	6.67	0.00	0.37	0.00	0.00	0.00	0.06	0.06	9.05
6	0.00	0.31	0.06	0.00	0.49	0.00	0.00	0.00	0.00	0.00	0.00	0.86
7	0.12	3.73	0.49	0.49	0.00	8.38	0.00	0.00	0.00	0.06	0.00	13.27
8	0.00	0.06	0.00	0.00	0.00	0.00	0.86	0.06	0.00	0.00	0.00	0.98
9	0.00	0.18	0.00	0.00	0.00	0.00	0.00	0.61	0.00	0.00	0.00	0.80
10	0.00	0.12	0.00	0.00	0.00	0.00	0.00	0.00	0.86	0.00	0.00	0.98
11	0.00	0.24	0.12	0.00	0.00	0.00	0.00	0.00	0.00	0.80	0.24	1.41
12	0.00	0.06	0.00	0.18	0.00	0.55	0.00	0.00	0.00	0.00	0.86	1.65
Sum	1.04	51.62	20.80	9.48	1.22	10.40	0.98	0.92	0.98	1.16	1.41	100.00
User's	0.6000	0.8418	0.7008	0.7365	0.5714	0.6313	0.8750	0.7692	0.8750	0.5652	0.5185	
Producer's	0.3529	0.7879	0.7441	0.7032	0.4000	0.8059	0.8750	0.6667	0.8750	0.6842	0.6087	
Overall	0.7602											

Table A21

Error matrix and accuracy assessment statistics for the KNN supervised classifier and study site A2. Unit labels: 2 – undulating bed, 4 – plain bed, 5 – plain bed with artefacts, 6 – other irregularities, 7 – uneven trough bed, 8 – linguoid (tongue-shaped) ripples, 9 – straight or sinuous ripples, 10 – groyne, 11 – submerged breakwaters, 12 – artificial reef modules, 13 – peat. Pred\Ref – Prediction\Reference.

Pred\Ref	2	4	5	6	7	9	10	11	12	13	Sum
2	3.29	2.17	0.00	0.13	0.72	0.00	0.13	0.00	0.13	0.20	6.77
4	2.50	54.60	4.99	0.26	2.17	0.26	0.20	0.13	0.46	0.13	65.70
5	0.13	2.89	10.84	0.00	0.07	0.00	0.00	0.07	0.00	0.00	13.99
6	0.00	0.13	0.00	0.53	0.07	0.07	0.00	0.00	0.00	0.00	0.79
7	0.39	2.23	0.00	0.07	4.53	0.46	0.26	0.00	0.00	0.26	8.21
9	0.13	0.07	0.00	0.00	0.20	0.20	0.00	0.00	0.00	0.00	0.59
10	0.07	0.00	0.00	0.00	0.07	0.00	0.33	0.07	0.00	0.00	0.53
11	0.00	0.07	0.00	0.00	0.07	0.00	0.00	1.91	0.00	0.07	2.10
12	0.00	0.00	0.00	0.00	0.00	0.00	0.07	0.20	0.59	0.00	0.85
13	0.07	0.00	0.00	0.00	0.20	0.00	0.00	0.00	0.00	0.20	0.46
Sum	6.57	62.16	15.83	0.99	8.08	0.99	0.99	2.37	1.18	0.85	100.00
User's	0.4854	0.8310	0.7746	0.6667	0.5520	0.3333	0.6250	0.9063	0.6923	0.4286	
Producer's	0.5000	0.8784	0.6846	0.5333	0.5610	0.2000	0.3333	0.8056	0.5000	0.2308	
Overall	0.7700										

Table A22

Error matrix and accuracy assessment statistics for the SVM supervised classifier and study site A2. Unit labels: 2 – undulating bed, 4 – plain bed, 5 – plain bed with artefacts, 6 – other irregularities, 7 – uneven trough bed, 8 – linguoid (tongue-shaped) ripples, 9 – straight or sinuous ripples, 10 – groyne, 11 – submerged breakwaters, 12 – artificial reef modules, 13 – peat. Pred\Ref – Prediction\Reference.

Pred\Ref	2	4	5	6	7	9	10	11	12	13	Sum
2	0.00	0.00	0.00	0.00	0.07	0.00	0.00	0.00	0.00	0.00	0.07
4	5.65	55.65	1.25	0.20	3.09	0.13	0.39	0.00	0.46	0.20	67.02
5	0.00	2.89	14.59	0.00	0.00	0.00	0.00	0.00	0.00	0.00	17.48
6	0.00	0.07	0.00	0.66	0.00	0.00	0.00	0.00	0.00	0.00	0.72
7	0.59	3.29	0.00	0.13	4.80	0.59	0.13	0.00	0.00	0.33	9.86
9	0.20	0.13	0.00	0.00	0.00	0.26	0.00	0.00	0.00	0.00	0.59
10	0.00	0.07	0.00	0.00	0.07	0.00	0.46	0.07	0.00	0.07	0.72
11	0.00	0.00	0.00	0.00	0.00	0.00	0.00	2.10	0.07	0.07	2.23
12	0.13	0.07	0.00	0.00	0.07	0.00	0.00	0.20	0.66	0.00	1.12
13	0.00	0.00	0.00	0.00	0.00	0.00	0.00	0.00	0.00	0.20	0.20
Sum	6.57	62.16	15.83	0.99	8.08	0.99	0.99	2.37	1.18	0.85	100.00
User's	0.0000	0.8304	0.8346	0.9091	0.4867	0.4444	0.6364	0.9412	0.5882	1.0000	
Producer's	0.0000	0.8953	0.9212	0.6667	0.5935	0.2667	0.4667	0.8889	0.5556	0.2308	
Overall	0.7937										

Table A23

Error matrix and accuracy assessment statistics for the CART supervised classifier and study site A2. Unit labels: 2 – undulating bed, 4 – plain bed, 5 – plain bed with artefacts, 6 – other irregularities, 7 – uneven trough bed, 8 – linguoid (tongue-shaped) ripples, 9 – straight or sinuous ripples, 10 – groyne, 11 – submerged breakwaters, 12 – artificial reef modules, 13 – peat. Pred\Ref – Prediction\Reference.

Pred\Ref	2	4	5	6	7	9	10	11	12	13	Sum
2	4.27	8.74	0.00	0.00	1.58	0.13	0.07	0.00	0.07	0.00	14.85
4	0.39	41.98	0.85	0.00	0.33	0.13	0.00	0.00	0.00	0.00	43.69
5	0.00	2.17	14.72	0.00	0.00	0.00	0.00	0.00	0.00	0.00	16.89
6	0.07	0.13	0.00	0.00	0.33	0.00	0.00	0.00	0.00	0.26	1.71
7	0.85	4.01	0.00	0.07	3.09	0.00	0.13	0.00	0.07	0.00	8.21
9	0.13	0.39	0.00	0.00	0.92	0.53	0.07	0.00	0.00	0.00	2.04
10	0.13	0.20	0.00	0.00	0.13	0.00	0.33	0.00	0.00	0.00	0.79
11	0.20	0.53	0.00	0.00	0.00	0.00	0.00	1.58	0.00	0.00	2.30
12	0.53	3.09	0.26	0.00	0.85	0.20	0.39	0.79	1.05	0.00	7.16
13	0.00	0.92	0.00	0.00	0.85	0.00	0.00	0.00	0.00	0.59	2.37
Sum	6.57	62.16	15.83	0.99	8.08	0.99	0.99	2.37	1.18	0.85	100.00
User's	0.2876	0.9609	0.8716	0.5385	0.3760	0.2581	0.4167	0.6857	0.1468	0.2500	
Producer's	0.6500	0.6755	0.9295	0.9333	0.3821	0.5333	0.3333	0.6667	0.8889	0.6923	
Overall	0.6905										

Table A24

Error matrix and accuracy assessment statistics for the RF supervised classifier and study site A2. Unit labels: 2 – undulating bed, 4 – plain bed, 5 – plain bed with artefacts, 6 – other irregularities, 7 – uneven trough bed, 8 – linguoid (tongue-shaped) ripples, 9 – straight or sinuous ripples, 10 – groyne, 11 – submerged breakwaters, 12 – artificial reef modules, 13 – peat. Pred\Ref – Prediction\Reference.

Pred\Ref	2	4	5	6	7	9	10	11	12	13	Sum
2	4.12	3.11	0.00	0.00	0.82	0.06	0.06	0.00	0.00	0.00	8.19
4	1.84	54.06	0.95	0.00	0.89	0.06	0.19	0.00	0.00	0.00	57.99
5	0.00	1.65	14.59	0.00	0.00	0.00	0.00	0.00	0.00	0.00	16.24
6	0.00	0.25	0.00	0.89	0.06	0.00	0.00	0.00	0.00	0.06	1.27
7	1.08	2.09	0.00	0.06	6.03	0.38	0.13	0.06	0.00	0.25	10.09
9	0.00	0.06	0.00	0.00	0.25	0.38	0.00	0.00	0.00	0.00	0.70
10	0.00	0.13	0.00	0.00	0.00	0.06	0.63	0.00	0.00	0.00	0.82
11	0.00	0.00	0.00	0.00	0.00	0.00	0.00	2.16	0.00	0.00	2.16
12	0.06	0.13	0.06	0.00	0.13	0.00	0.00	0.06	1.14	0.00	1.59
13	0.00	0.00	0.00	0.00	0.32	0.00	0.00	0.00	0.00	0.63	0.95
Sum	7.11	61.48	15.61	0.95	8.50	0.95	1.02	2.28	1.14	0.95	100.00
User's	0.5039	0.9322	0.8984	0.7000	0.5975	0.5455	0.7692	1.0000	0.7200	0.6667	
Producer's	0.5804	0.8793	0.9350	0.9333	0.7090	0.4000	0.6250	0.9444	1.0000	0.6667	
Overall	0.8464										

Table A25

Error matrix and accuracy assessment statistics for the RF supervised classifier and 48 km of the nearshore area, model G1. Unit labels: 1 – artefacts, 2 – undulating bed, 3 – undulating bed with artefacts, 4 – plain bed, 5 – plain bed with artefacts, 6 – other irregularities, 7 – uneven trough bed, 8 – linguoid (tongue-shaped) ripples, 9 – straight or sinuous ripples. Pred\Ref – Prediction\Reference.

Pred\Ref	1	2	3	4	5	6	7	8	9	Sum
1	0.73	0.00	0.00	0.02	0.12	0.00	0.00	0.00	0.02	0.89
2	0.02	9.25	0.00	0.59	0.00	0.00	0.00	0.00	0.20	10.06
3	0.10	0.18	15.13	0.22	0.85	0.00	0.00	0.00	0.00	16.49
4	0.00	0.22	0.00	27.03	0.00	0.00	0.00	0.04	0.28	27.58
5	0.69	0.63	0.20	6.90	3.75	0.00	0.57	0.00	0.49	13.22
6	0.28	0.02	0.00	2.90	0.00	1.85	0.00	0.16	0.00	5.21
7	0.18	0.06	0.00	0.02	0.00	0.00	2.41	0.00	0.14	2.82
8	0.06	0.00	0.00	0.22	0.00	0.00	0.00	4.77	0.14	5.19
9	0.28	1.16	0.00	0.83	0.08	0.00	0.14	0.02	16.02	18.54
Sum	2.35	11.52	15.33	38.73	4.81	1.85	3.12	4.99	17.30	100.00
User's	0.8182	0.9194	0.9176	0.9801	0.2837	0.3541	0.8561	0.9180	0.8643	
Producer's	0.3103	0.8028	0.9868	0.6979	0.7806	1.0000	0.7727	0.9553	0.9261	
Overall	0.8094									

Table A26

Error matrix and accuracy assessment statistics for the RF supervised classifier and the 48 km of the nearshore area, model G2. Unit labels: 1 – artefacts, 2 – undulating bed, 3 – undulating bed with artefacts, 4 – plain bed, 5 – plain bed with artefacts, 6 – other irregularities, 7 – uneven trough bed, 8 – linguoid (tongue-shaped) ripples, 9 – straight or sinuous ripples. Pred\Ref – Prediction\Reference.

Pred/Ref	1	2	3	4	5	6	7	8	9	Sum
1	0.60	0.02	0.00	0.00	0.23	0.00	0.02	0.00	0.00	0.87
2	0.10	11.64	0.00	0.58	0.66	0.00	0.08	0.00	0.14	13.20
3	0.00	0.00	1.16	0.00	0.04	0.00	0.00	0.00	0.00	1.20
4	0.00	0.25	0.00	18.14	0.91	0.00	0.06	0.00	0.23	19.60
5	0.89	2.72	0.12	1.36	26.22	0.00	0.43	0.00	0.47	32.19
6	0.25	0.12	0.00	0.23	0.00	13.56	0.00	0.39	0.00	14.55
7	0.31	0.10	0.00	0.52	0.78	0.00	10.07	0.00	0.12	11.90
8	0.00	0.00	0.00	0.00	0.00	0.00	0.00	0.37	0.00	0.37
9	0.19	0.10	0.00	0.10	1.96	0.00	0.27	0.00	3.49	6.11
Sum	2.35	14.94	1.28	20.94	30.80	13.56	10.93	0.76	4.44	100.00
User's	0.6889	0.8824	0.9677	0.9257	0.8143	0.9320	0.8467	1.0000	0.5714	
Producer's	0.2562	0.7792	0.9091	0.8665	0.8513	1.0000	0.9218	0.4872	0.7860	
Overall	0.8527									

Table A27

Error matrix and accuracy assessment statistics for the RF supervised classifier and study site N1. Unit labels: 1 – artefacts, 2 – undulating bed, 4 & 5 – plain bed and plain bed with artefacts, 6 – other irregularities, 7 – uneven trough bed, 8 – linguoid (tongue-shaped) ripples, 9 – straight or sinuous ripples. Pred\Ref – Prediction\Reference.

Pred/Ref	1	2	4 & 5	6	8	9	Sum
1	1.59	0.20	0.07	0.00	0.00	0.13	1.98
2	0.07	3.04	0.33	0.00	0.07	0.40	3.90
4 & 5	0.13	1.46	69.31	0.07	0.00	0.53	71.49
6	0.00	0.26	0.20	1.85	0.07	0.00	2.38
8	0.00	0.07	0.00	0.20	1.59	0.00	1.85
9	0.40	0.73	0.86	0.00	0.00	16.40	18.39
Sum	2.18	5.75	70.77	2.12	1.72	17.46	100.00
User's	0.8000	0.7797	0.9695	0.7778	0.8571	0.8921	
Producer's	0.7273	0.5287	0.9794	0.8750	0.9231	0.9394	
Overall	0.9378						

Table A28

Error matrix and accuracy assessment statistics for the RF supervised classifier and study site N2. Unit labels: 2 & 3 – undulating bed and undulating bed with artefacts, 4&5 – plain bed and plain bed with artefacts, 6 – other irregularities, 7 – uneven trough bed, 8 – linguoid (tongue-shaped) ripples, 9 – straight or sinuous ripples. Pred\Ref – Prediction\Reference.

Pred/Ref	2 & 3	4 & 5	6	7	8	9	Sum
2 & 3	23.27	2.80	0.00	0.21	0.00	1.05	27.33
4 & 5	2.73	37.84	0.00	0.35	0.49	0.91	42.33
6	0.00	0.42	1.89	0.00	0.07	0.00	2.38
7	0.49	0.56	0.00	1.75	0.00	0.14	2.94
8	0.00	0.98	0.00	0.00	4.48	1.05	6.52
9	1.89	1.40	0.00	0.14	0.14	14.93	18.50
Sum	28.38	44.01	1.89	2.45	5.19	18.08	100.00
User's	0.8513	0.894	0.7941	0.5952	0.6882	0.8068	
Producer's	0.8198	0.8599	1.0000	0.7143	0.8649	0.8256	
Overall	0.8416						

Table A29

Error matrix and accuracy assessment statistics for the RF supervised classifier and study site N3. Unit labels: 2 & 3 – undulating bed and undulating bed with artefacts, 4 & 5 – plain bed and plain bed with artefacts, 6 – other irregularities, 7 – uneven trough bed, 8 – linguoid (tongue-shaped) ripples, 9 – straight or sinuous ripples. Pred\Ref – Prediction\Reference.

Pred/Ref	2 & 3	4 & 5	6	7	8	9	Sum
2 + 3	10.99	1.55	0.13	0.47	0.00	0.27	13.42
4 + 5	1.75	49.63	0.00	1.08	0.00	0.27	52.73
6	0.20	0.07	14.03	0.00	0.40	0.00	14.70
7	0.81	1.96	0.00	9.98	0.00	0.40	13.15
8	0.00	0.00	0.00	0.00	0.13	0.00	0.13
9	1.69	0.34	0.00	0.34	0.00	3.51	5.87
Sum	15.44	53.54	14.16	11.87	0.54	4.45	100.00

(continued on next page)

Table A29 (continued)

Pred/Ref	2 & 3	4 & 5	6	7	8	9	Sum
User's	0.8191	0.9412	0.9541	0.7590	1.0000	0.5977	
Producer's	0.7118	0.9270	0.9905	0.8409	0.2500	0.7879	
Overall	0.8827						

Table A30

Error matrix and accuracy assessment statistics for the RF supervised classifier and study site N4. Unit labels: 1 – artefacts, 2 – undulating bed, 4 & 5 – plain bed and plain bed with artefacts, 6 – other irregularities, 7 – uneven trough bed, 8 – linguoid (tongue-shaped) ripples, 9 – straight or sinuous ripples. Pred\Ref – Prediction\Reference.

Pred/Ref	1	2	4 & 5	6	7	9	Sum
1	2.93	0.00	2.02	0.20	0.07	0.00	5.22
2	0.00	4.56	1.24	0.26	0.00	0.07	6.13
4 + 5	1.89	2.93	60.89	0.07	0.59	0.33	66.69
6	0.72	0.46	0.46	13.17	0.00	0.46	15.25
7	0.07	0.07	0.65	0.13	2.74	0.26	3.91
9	0.07	0.20	1.11	0.00	0.07	1.37	2.80
Sum	5.67	8.21	66.36	13.82	3.46	2.48	100.00
User's	0.5625	0.7447	0.9130	0.8632	0.7000	0.4884	
Producer's	0.5172	0.5556	0.9175	0.9528	0.7925	0.5526	
Overall	0.8566						

Table A31

Error matrix and accuracy assessment statistics for the RF supervised classifier and study site A1. Unit labels: 1 – artefacts, 2 – undulating bed, 4 & 5 – plain bed and plain bed with artefacts, 6 – other irregularities, 7 – uneven trough bed, 8 – linguoid (tongue-shaped) ripples, 9 – straight or sinuous ripples, 10 – groyne, 11 – submerged breakwaters, 12 – artificial reef modules. Pred\Ref – Prediction\Reference.

Pred/Ref	1	2	4 & 5	6	7	8	9	10	11	12	Sum
1	0.37	0.18	0.00	0.00	0.06	0.00	0.00	0.00	0.00	0.00	0.61
2	0.43	40.67	5.50	0.24	0.92	0.06	0.12	0.12	0.18	0.06	48.32
4 + 5	0.12	6.06	23.43	0.49	0.49	0.06	0.12	0.00	0.12	0.24	31.13
6	0.00	0.31	0.06	0.49	0.00	0.00	0.00	0.00	0.00	0.00	0.86
7	0.12	3.73	0.98	0.00	8.38	0.00	0.00	0.00	0.06	0.00	13.27
8	0.00	0.06	0.00	0.00	0.00	0.86	0.06	0.00	0.00	0.00	0.98
9	0.00	0.18	0.00	0.00	0.00	0.00	0.61	0.00	0.00	0.00	0.80
10	0.00	0.12	0.00	0.00	0.00	0.00	0.00	0.86	0.00	0.00	0.98
11	0.00	0.24	0.12	0.00	0.00	0.00	0.00	0.00	0.80	0.24	1.41
12	0.00	0.06	0.18	0.00	0.55	0.00	0.00	0.00	0.00	0.86	1.65
Sum	1.04	51.62	30.28	1.22	10.40	0.98	0.92	0.98	1.16	1.41	100.00
User's	0.6000	0.8418	0.7525	0.5714	0.6313	0.8750	0.7692	0.8750	0.5652	0.5185	
Producer's	0.3529	0.7879	0.7737	0.4000	0.8059	0.8750	0.6667	0.8750	0.6842	0.6087	
Overall	0.7731										

Table A32

Error matrix and accuracy assessment statistics for the RF supervised classifier and study site A2. Unit labels: 2 – undulating bed, 4 & 5 – plain bed and plain bed with artefacts, 6 – other irregularities, 7 – uneven trough bed, 8 – linguoid (tongue-shaped) ripples, 9 – straight or sinuous ripples, 10 – groyne, 11 – submerged breakwaters, 12 – artificial reef modules, 13 – peat. Pred\Ref – Prediction\Reference.

Pred/Ref	2	4 & 5	6	7	9	10	11	12	13	Sum
2	4.12	3.11	0.00	0.82	0.06	0.06	0.00	0.00	0.00	8.19
4 + 5	1.84	71.26	0.00	0.89	0.06	0.19	0.00	0.00	0.00	74.24
6	0.00	0.25	0.89	0.06	0.00	0.00	0.00	0.00	0.06	1.27
7	1.08	2.09	0.06	6.03	0.38	0.13	0.06	0.00	0.25	10.09
9	0.00	0.06	0.00	0.25	0.38	0.00	0.00	0.00	0.00	0.70
10	0.00	0.13	0.00	0.00	0.06	0.63	0.00	0.00	0.00	0.82
11	0.00	0.00	0.00	0.00	0.00	0.00	2.16	0.00	0.00	2.16
12	0.06	0.19	0.00	0.13	0.00	0.00	0.06	1.14	0.00	1.59
13	0.00	0.00	0.00	0.32	0.00	0.00	0.00	0.00	0.63	0.95
Sum	7.11	77.09	0.95	8.50	0.95	1.02	2.28	1.14	0.95	100.00
User's	0.5039	0.9598	0.7000	0.5975	0.5455	0.7692	1.0000	0.7200	0.6667	
Producer's	0.5804	0.9243	0.9333	0.7090	0.4000	0.6250	0.9444	1.0000	0.6667	
Overall	0.8725									

Table A33

Error matrix and accuracy assessment statistics for the RF supervised classifier and the 48 km of the nearshore area, model G1. Unit labels: 1 – artefacts, 2 & 3 – undulating bed and undulating bed with artefacts, 4 & 5 – plain bed and plain bed with artefacts, 6 – other irregularities, 7 – uneven trough bed, 8 – linguoid (tongue-shaped) ripples, 9 – straight or sinuous ripples. Pred\Ref – Prediction\Reference.

Pred/Ref	1	2 & 3	4 & 5	6	7	8	9	Sum
1	0.73	0.00	0.14	0.00	0.00	0.00	0.02	0.89
2 + 3	0.12	24.56	1.66	0.00	0.00	0.00	0.20	26.55
4 + 5	0.69	1.05	37.68	0.00	0.57	0.04	0.77	40.80
6	0.28	0.02	2.90	1.85	0.00	0.16	0.00	5.21
7	0.18	0.06	0.02	0.00	2.41	0.00	0.14	2.82
8	0.06	0.00	0.22	0.00	0.00	4.77	0.14	5.19
9	0.28	1.16	0.91	0.00	0.14	0.02	16.02	18.54
Sum	2.35	26.85	43.54	1.85	3.12	4.99	17.30	100.00
User's	0.8182	0.9251	0.9235	0.3541	0.8561	0.9180	0.8643	
Producer's	0.3103	0.9147	0.8654	1.0000	0.7727	0.9553	0.9261	
Overall	0.8801							

Table A34

Error matrix and accuracy assessment statistics for the RF supervised classifier and the 48 km of the nearshore area, model G2. Unit labels: 1 – artefacts, 2 & 3 – undulating bed and undulating bed with artefacts, 4 & 5 – plain bed and plain bed with artefacts, 6 – other irregularities, 7 – uneven trough bed, 8 – linguoid (tongue-shaped) ripples, 9 – straight or sinuous ripples. Pred\Ref – Prediction\Reference.

Pred/Ref	1	2 & 3	4 & 5	6	7	8	9	Sum
1	0.60	0.02	0.23	0.00	0.02	0.00	0.00	0.87
2 + 3	0.10	12.81	1.28	0.00	0.08	0.00	0.14	14.40
4 + 5	0.89	3.09	46.63	0.00	0.49	0.00	0.70	51.80
6	0.25	0.12	0.23	13.56	0.00	0.39	0.00	14.55
7	0.31	0.10	1.30	0.00	10.07	0.00	0.12	11.90
8	0.00	0.00	0.00	0.00	0.00	0.37	0.00	0.37
9	0.19	0.10	2.06	0.00	0.27	0.00	3.49	6.11
Sum	2.35	16.22	51.74	13.56	10.93	0.76	4.44	100.00
User's	0.6889	0.8895	0.9003	0.9320	0.8467	1.0000	0.5714	
Producer's	0.2562	0.7895	0.9014	1.0000	0.9218	0.4872	0.7860	
Overall	0.8754							

References

- Andersen, M.S., Gergely, Á., Al-Hamdani, Z., Steinbacher, F., Larsen, L.R., Ernsten, V.B., 2017. Processing and performance of topobathymetric lidar data for geomorphometric and morphological classification in a high-energy tidal environment. *Hydrol. Earth Syst. Sci.* 21, 43–63. <https://doi.org/10.5194/hess-21-43-2017>.
- Benz, U.C., Hofmann, P., Willhauck, G., Lingenfelder, I., Heynen, M., 2004. Multi-resolution, object-oriented fuzzy analysis of remote sensing data for GIS-ready information. *ISPRS J. Photogramm. Remote Sens.* 58, 239–258. <https://doi.org/10.1016/j.isprsjprs.2003.10.002>.
- Blaschke, T., 2010. Object based image analysis for remote sensing. *ISPRS J. Photogramm. Remote Sens.* 65, 2–16. <https://doi.org/10.1016/j.isprsjprs.2009.06.004>.
- Breiman, L., 2001. Random Forests. *Mach. Learn.* 45, 5–32. <https://doi.org/10.1023/a:1010933404324>.
- Breiman, L., Friedman, J.H., Olshen, R.A., Stone, C.J., 1984. *Classification and Regression Trees*. Wadsworth, Belmont.
- Brown, C.J., Smith, S.J., Lawton, P., Anderson, J.T., 2011. Benthic habitat mapping: a review of progress towards improved understanding of the spatial ecology of the seafloor using acoustic techniques. *Estuar. Coast. Shelf Sci.* 92, 502–520. <https://doi.org/10.1016/j.ecss.2011.02.007>.
- Chen, G., Weng, Q., Hay, G.J., He, Y., 2018. Geographic object-based image analysis (GEOBIA): emerging trends and future opportunities. *GIScience & Remote Sensing* 55, 159–182. <https://doi.org/10.1080/15481603.2018.1426092>.
- Collin, A., Archambault, P., Long, B., 2008. Mapping the Shallow Water Seabed Habitat with the SHOALS. *IEEE Trans. Geosci. Remote Sens.* 46, 2947–2955. <https://doi.org/10.1109/tgrs.2008.920020>.
- Cottin, A.G., Forbes, D.L., Long, B.F., 2014. Shallow seabed mapping and classification using waveform analysis and bathymetry from SHOALS lidar data. *Can. J. Remote Sens.* 35, 422–434. <https://doi.org/10.5589/m09-036>.
- Coveney, S., Monteys, X., 2011. Integration potential of INFOMAR Airborne LIDAR Bathymetry with External Onshore LIDAR Data Sets. *J. Coast. Res.* 62, 19–29. <https://doi.org/10.2112/si.62.3>.
- Diesing, M., Mitchell, P., Stephens, D., 2016. Image-based seabed classification: what can we learn from terrestrial remote sensing? *ICES J. Marine Sci.: J. du Conseil* 73, 2425–2441. <https://doi.org/10.1093/icesjms/fsw118>.
- Dolan, M.F.J., Ross, R.E., Albreten, J., Skarðhamar, J., Gonzalez-Mirelis, G., Bellec, V.K., Buhl-Mortensen, P., Bjarnadóttir, L.R., 2021. Using spatial validity and uncertainty metrics to determine the relative suitability of alternative suites of oceanographic data for seabed biotope prediction. A case study from the Barents Sea, Norway. *Geosciences* 11. <https://doi.org/10.3390/geosciences11020048>.
- Doneus, M., Miholjek, I., Mandlbürger, G., Doneus, N., Verhoeven, G., Briese, C., Pregelbauer, M., 2015. Airborne Laser Bathymetry for Documentation of Submerged Archaeological Sites in Shallow Water. In: *The International Archives of the Photogrammetry, Remote Sensing and Spatial Information Sciences*, XL-5/W5, pp. 99–107. <https://doi.org/10.5194/isprsarchives-XL-5-W5-99-2015>.
- Dubrawski, R., Zawadzka-Kahlau, E., 2006. *Przyszłość ochrony polskich brzegów morskich*. Zakład Wydawnictw Naukowych Instytutu Morskiego, Gdańsk.
- Fogarin, S., Madricardo, F., Zaggia, L., Sigovini, M., Montereale-Gavazzi, G., Kruss, A., Lorenzetti, G., Manfè, G., Petrizzo, A., Molinaroli, E., Trincardi, F., 2019. Tidal inlets in the Anthropocene: geomorphology and benthic habitats of the Chioggia inlet, Venice Lagoon (Italy). *Earth Surf. Process. Landf.* 44, 2297–2315. <https://doi.org/10.1002/esp.4642>.
- Foody, G.M., 2002. Status of land cover classification accuracy assessment. *Remote Sens. Environ.* 80, 185–201. [https://doi.org/10.1016/S0034-4257\(01\)00295-4](https://doi.org/10.1016/S0034-4257(01)00295-4).
- Gallant, J.C., Dowling, T.I., 2003. A multiresolution index of valley bottom flatness for mapping depositional areas. *Water Resour. Res.* 39 <https://doi.org/10.1029/2002wr001426>.
- Genchi, S.A., Vitale, A.J., Perillo, G.M., Delrieux, C.A., 2015. Structure-from-motion approach for characterization of bioerosion patterns using UAV imagery. *Sensors (Basel)* 15, 3593–3609. <https://doi.org/10.3390/s150203593>.
- Guo, K., Li, Q., Mao, Q., Wang, C., Zhu, J., Liu, Y., Xu, W., Zhang, D., Wu, A., 2021. Errors of Airborne Bathymetry LiDAR Detection Caused by Ocean Waves and Dimension-based Laser Incidence Correction. *Remote Sens.* 13 <https://doi.org/10.3390/rs13091750>.
- Janowski, L., Wroblewski, R., Dworniczak, J., Kolakowski, M., Rogowska, K., Wojcik, M., Gajewski, J., 2021. Offshore benthic habitat mapping based on object-based image analysis and geomorphometric approach. A case study from the Slupsk Bank, Southern Baltic Sea. *Sci. Total Environ.* 801, 149712 <https://doi.org/10.1016/j.scitotenv.2021.149712>.
- Kaszubowski, L., Coufal, R., 2010. Preliminary geological division of the polish Baltic seabed. *Inżynieria Morska i Geotechnika* 31, 392–401.
- Kundzewicz, Z.W., Piniewski, M., Mezghani, A., Okruszko, T., Pińskwar, I., Kardel, I., Hov, Ø., Szcześniak, M., Szwed, M., Benestad, R.E., Marcinkowski, P., Graczyk, D., Dobler, A., Forland, E.J., O'Keefe, J., Choryński, A., Parding, K.M., Haugen, J.E.,

2018. Assessment of climate change and associated impact on selected sectors in Poland. *Acta Geophysica* 66, 1509–1523. <https://doi.org/10.1007/s11600-018-0220-4>.
- Kursa, M.B., Rudnicki, W.R., 2016. Package 'Boruta'. Wrapper Algorithm for All Relevant Feature Selection.
- Kutser, T., Miller, I., Jupp, D.L.B., 2006. Mapping coral reef benthic substrates using hyperspectral space-borne images and spectral libraries. *Estuar. Coast. Shelf Sci.* 70, 449–460. <https://doi.org/10.1016/j.ecss.2006.06.026>.
- Lague, D., Feldmann, B., 2020. Chapter 2 - Topo-bathymetric airborne LiDAR for fluvial-geomorphology analysis. In: Tarolli, P., Mudd, S.M. (Eds.), *Developments in Earth Surface Processes*. Elsevier, pp. 25–54.
- Long, B., Aucoin, F., Montreuil, S., Robitaille, V., Xhardé, R., 2011. Airborne Lidar Bathymetry Applied to Coastal Hydrodynamic Processes. *Coastal Engineering Proceedings* 1. <https://doi.org/10.9753/icce.v32.sediment.26>.
- Lucieer, V.L., 2008. Object-oriented classification of sidescan sonar data for mapping benthic marine habitats. *Int. J. Remote Sens.* 29, 905–921. <https://doi.org/10.1080/01431160701311309>.
- Maritime Office in Gdynia, 2020. Monitoring of the seashores. World Wide Web Address. <https://www.mediafire.com/folder/u9519197wjsiv/Monitoring#u9519197wjsiv>.
- Musielak, S., Furmańczyk, K., Bugajny, N., 2017. Factors and Processes Forming the Polish Southern Baltic Sea Coast on various Temporal and Spatial Scales. In: Harff, J., Furmańczyk, K., von Storch, H. (Eds.), *Coastline Changes of the Baltic Sea from South to East: Past and Future Projection*. Springer International Publishing, Cham, pp. 69–85.
- Ossowski, R., Przyborski, M., Tysiac, P., 2019. Stability Assessment of Coastal Cliffs Incorporating Laser Scanning Technology and a Numerical Analysis. *Remote Sens.* 11 <https://doi.org/10.3390/rs11161951>.
- Prampolini, M., Angeletti, L., Castellani, G., Grande, V., Le Bas, T., Taviani, M., Fogliani, F., 2021. Benthic Habitat Map of the Southern Adriatic Sea (Mediterranean Sea) from Object-based image Analysis of Multi-Source Acoustic Backscatter Data. *Remote Sens.* 13, 2913. <https://doi.org/10.3390/rs13152913>.
- Pruszk, Z., Zawadzka, E., 2008. Potential Implications of Sea-Level rise for Poland. *J. Coast. Res.* 242, 410–422. <https://doi.org/10.2112/07a-0014.1>.
- Reusch, T.B.H., Dierking, J., Andersson, H.C., Bonsdorff, E., Carstensen, J., Casini, M., Czajkowski, M., Hasler, B., Hinsby, K., Hyytiäinen, K., Johannesson, K., Jomaa, S., Jormalainen, V., Kuosa, H., Kurland, S., Laikre, L., MacKenzie, B.R., Margonski, P., Melzner, F., Oesterwind, D., Ojaveer, H., Refsgaard, J.C., Sandström, A., Schwarz, G., Tonderski, K., Winder, M., Zandersen, M., 2018. The Baltic Sea as a time machine for the future coastal ocean. *Sci. Adv.* 4, eaar8195. <https://doi.org/10.1126/sciadv.aar8195>.
- Riegl, 2019. Datasheet Riegl VQ-1560i-DW. World Wide Web Address. http://www.riegl.com/uploads/tx_pxpriegidownloads/RIEGL_VQ-1560i-DW_Datasheet_2019-09-02.pdf.
- Robertson, Q., Dunkin, L., Dong, Z., Wozencraft, J., Zhang, K., 2018. Florida and US East Coast Beach Change Metrics Derived from LiDAR Data Utilizing ArcGIS Python based Tools. In: Botero, C.M., Cervantes, O., Finkl, C.W. (Eds.), *Beach Management Tools - Concepts, Methodologies and Case Studies*. Springer International Publishing, Cham, pp. 239–258.
- Schmidt, A., Rottensteiner, F., Soergel, U., 2013. Monitoring Concepts for Coastal areas using Lidar Data. *International Archives of the Photogrammetry, Remote Sensing and Spatial. Inf. Sci.* XL-1/W1, 311–316.
- Turner, J.A., Babcock, R.C., Hovey, R., Kendrick, G.A., 2018. Can single classifiers be as useful as model ensembles to produce benthic seabed substratum maps? *Estuar. Coast. Shelf Sci.* 204, 149–163. <https://doi.org/10.1016/j.ecss.2018.02.028>.
- Tysiac, P., 2020. Bringing Bathymetry LiDAR to Coastal Zone Assessment: a Case Study in the Southern Baltic. *Remote Sens.* 12 <https://doi.org/10.3390/rs12223740>.
- Uścińowicz, S., 2011. Geochemistry of Baltic Sea Surface Sediments. Polish Geological Institute-National Research Institute, Warsaw.
- Wehr, A., Lohr, U., 1999. Airborne laser scanning—an introduction and overview. *ISPRS J. Photogramm. Remote Sens.* 54, 68–82. [https://doi.org/10.1016/S0924-2716\(99\)00011-8](https://doi.org/10.1016/S0924-2716(99)00011-8).
- Wozencraft, J., Millar, D., 2005. Airborne Lidar and Integrated Technologies for Coastal Mapping and Nautical Charting. *Mar. Technol. Soc. J.* 39.
- Xhardé, R., Long, B.F., Forbes, D.L., 2011. Short-Term Beach and Shoreface Evolution on a Cuspate Foreland Observed with Airborne Topographic and Bathymetric LiDAR. *J. Coast. Res.* 62, 50–61. https://doi.org/10.2112/si_62.6.